nature communications

Article

https://doi.org/10.1038/s41467-024-55164-3

Aging-induced immune microenvironment remodeling fosters melanoma in male mice via γδ17-Neutrophil-CD8 axis

Received: 6 February 2024

Accepted: 28 November 2024

Published online: 30 December 2024

Check for updates

Runping Duan[1,4], Loujing Jiang[1,4], Tianfu Wang[1,4], Zhaohuai Li[1], Xiaoyang Yu[2], Yuehan Gao[1], Renbing Jia[3,5] ✉, Xianqun Fan[3,5] ✉ & Wenru Su[1,3,5] ✉

Aging is associated with increased tumor metastasis and poor prognosis. However, how an aging immune system contributes to the process is unclear. Here, single-cell RNA sequencing reveals that in male mice, aging shifts the lung immune microenvironment towards a premetastatic niche, characterized by an increased proportion of IL-17-expressing γδT (γδ17) and neutrophils. Mechanistically, age-dependent downregulation of the immune trafficking receptor S1pr1 drives the expansion of γδ17. Compared to young mice, expanded γδ17 recruit tumor-promoting neutrophils with lower expression levels of CD62L and higher levels of C-kit and CXCR4. These neutrophils suppress the stemness and tumor-killing functions of CD8+ T cells in aged male mice. Accordingly, antibody-mediated depletion of γδT or neutrophils reduces tumor metastatic foci in aged animals, and the administration of the senolytic agent procyanidin C1 reverses the observed immune-mediated, tumor-promoting effects of aging. Thus, we uncover a γδ17-Neutrophil-CD8 axis that promotes aging-driven tumor metastasis in male mice and provides potential insights for managing metastatic tumors.

Cancer is a principal cause of death worldwide, and population aging is a vital determinant of most cancer-related deaths. Approximately half of all new cancer cases are diagnosed in adults older than 65 years, and this ratio is expected to increase in the future with the elderly population becoming larger. More importantly, cancer patients mainly die from metastasis rather than the primary tumor due to the higher likelihood of developing invasive cancer in patients older than 60 years compared to younger patients[1,2]. However, the role of aging on tumor metastasis is still inconclusive. Cancer and aging share several characteristics such as genomic instability and chronic inflammation[3]; meanwhile, certain types of cancers are more aggressive when diagnosed in younger patients[4]. Given the expanding aged population and the World Health Organization's prediction that up to 16% of the population will be over 65 years of age by 2050, further studies are needed to explore the impact of aging on cancer metastasis and progression.

Immune surveillance is indispensable for preventing tumor escape and suppressing cancer metastasis, and aging has been found to significantly undermine this aspect of the immune system[1,4]. Studies have shown that the immune system enters a systemic low-grade chronic inflammation state, known as "inflamm-aging", when aging progresses[5]. This persistent inflammatory condition not only causes tissue degeneration and dysfunction, but it is also highly correlated with tumor metastasis[6]. Additionally, other age-related immune system alterations are also long noticed, including immunosenescence and the increase in immunosuppressive cell populations[7]. Our previous studies[8,9] revealed that aging reduces both naïve and memory T cells and polarizes them into effector, cytotoxic, exhausted, and

[1]State Key Laboratory of Ophthalmology, Zhongshan Ophthalmic Center, Sun Yat-sen University, Guangdong Provincial Key Laboratory of Ophthalmology and Visual Science, Guangzhou 510060, China. [2]Guangzhou University of Chinese Medicine, Guangzhou 510060, China. [3]Department of Ophthalmology, Ninth People's Hospital, Shanghai Jiao Tong University School of Medicine, Shanghai, China. [4]These authors contributed equally: Runping Duan, Loujing Jiang, Tianfu Wang. [5]These authors jointly supervised this work: Renbing Jia, Xianqun Fan, Wenru Su. ✉e-mail: renbingjia@sjtu.edu.cn; fanxq@sjtu.edu.cn; swrth@163.com

regulatory cells. Meanwhile, the expression of a cluster of inflammation-related genes was globally upregulated. These studies explored systemic immune alterations during aging; however, the impact of aging on modulating the local immune microenvironment and ultimately influencing tumor metastasis has not been fully investigated.

Malignant melanoma is a highly aggressive type of cancer characterized by an escalating incidence and a relatively high tendency to metastasize. This cancer affects primarily older individuals and aging is an indicator of its poor prognosis[10]. Unfortunately, current studies mostly utilize young animal models, which possess distinguished tumor immune microenvironment from the older individuals. This discrepancy may at least partially explain the gap of the results between the animal model and the patients.

In this work, we reveal that aging promotes metastasis of melanoma in male mice. Based on the classical melanoma lung metastasis model, we construct a comprehensive single-cell atlas of the local immune microenvironment of lung tissue in young and aged mice with and without tumor burden. Furthermore, we uncover that aging hampers the tumor-killing capacity of CD8+ T cells through the γδ17-Neutrophil-CD8 axis, which ultimately facilitates tumor metastasis. Additionally, the administration of procyanidin C1 (PCC1), a kind of senolytic agents, ameliorates the impact of aging. Our findings elucidate the role of the aged immune microenvironment in eliciting a premetastatic niche and targeting the γδ17-Neutrophil-CD8 axis, which represents an effective strategy to inhibit tumor metastasis.

Results

Aging result significant alteration in tissue-resident immune cell

To understand the role of aging in the pathogenesis of melanoma, we adopted a lung metastatic tumor model[11] by injecting B16F10 cells into the tail veins of both young and old C57BL/6J mice. Compared to the young mice, we observed three-fold increase in the number of pulmonary metastatic foci in the aged mice three weeks after injection (Fig. 1a). This observation was further validated by hematoxylin-eosin staining (Supplementary Fig. 1a). Since melanoma also occurs in choroid, we compared the metastasis pattern between the older and young mice in an orthotopic ocular melanoma model by subretinal injection[12]. Shown in Fig. 1b, intraocular tumors formed in both young and old mice. The number of liver micrometastatic foci was significantly higher in the aged mice, suggesting that aging promotes metastasis.

We speculated that the above phenomenon was due to altered immune microenvironment by aging. To test such speculation and further uncover the underlying mechanism, we generated single-cell RNA-seq (scRNA-seq) profiles of the lung tissue-resident immune cells from four groups of mice, including young control (YC), aged control (AC), young model (YM) and aged model (AM) mice. The model group was injected with B16F10 cells via the tail vein to establish the aforementioned lung metastasis, while the control group was not inoculated with tumor cells. The graphic presentation of experiment procedures is shown in Fig. 1c, highly purified immune cells in lung tissue were sorted for the following scRNA-seq (Supplementary Fig. 1b). No batch effect was seen between the four groups after correction with Harmony (Supplementary Fig. 1c). Based on the expression of classical lineage markers[11], we identified five major immune cell lineages (Fig. 1d and Supplementary Fig. 1d, e), including T cells, B cells, natural killer cells (NK), neutrophils, monocytes as well as "macrophages and dendritic cells" (MOMøDC).

We firstly examined the effects of aging on YC and AC groups. Aging increased the proportion of neutrophil, decreased the proportion of B cells and NK, and had less effect on MOMøDC (Fig. 1d). To determine the aging-associated gene expression signature, we further analyzed differentially expressed genes (DEG) of all immune cells between YC and AC mice (Fig. 1e). We noticed that the inflammatory factors *S100a8*, *S100a9*, *Il1b*, and the activation marker *Cd44* were among the upregulated DEGs. S100a8 and S100a9 are known to frequently exist as homodimers and function as chemotactic factors in neutrophils. They have also been reported to be important components of the premetastatic niche[13]. Il1b induces metastasis through IL-17 stimulation. Some melanoma metastasis-associated genes such as *Cxcr2*, *Mmp9* and *Tgfbi* were also upregulated in AC mice. The downregulated genes in AC mice included the naïve phenotype-associated gene *Ccr7*, combined with a higher expression level of the activation marker *Cd44* (Fig. 1e), probably indicating that aging results in immune cells with a polarized phenotype[8]. These genes were also upregulated or downregulated in various cell types (Supplementary Fig. 1f, g). Consistent with the largest change observed in neutrophils population, the Gene Ontology (GO) and pathway analyses showed a series of neutrophil-related pathways including degranulation, migration, chemotaxis and activation among the upregulated pathways. The inflammatory response and positive regulation of angiogenesis pathway were also upregulated (Fig. 1f). Interestingly, Il-17 signaling pathway was identified as one of the major interleukin pathways. In consistency with the decreased B cell population in AC mice, among downregulated pathways (Fig. 1g) are lymphocyte-associated including lymphocyte differentiation, signaling by the B cell receptor, antigen processing and presentation, together with translation-associated pathways (ribosomal large subunit assembly, translational initiation). Since translation is among the top list for energy consumption, its downregulation may reflect the reduction of energy production, synergized by downregulated cellular respiration. Generally, decreased energy metabolism is a phenomenon known in aging. In addition, the T cell-related pathways are among those downregulated signaling, indicating their functional changes. We also calculated the scores of several inflammation-related pathways, which showed increased abundance across multiple cell types with aging (Supplementary Fig. 1h). In B cells and NK cells (both ratios decreased), we also observed an increase in inflammation-related pathways such as inflammatory response and IL-17 signaling pathway, along with a decline in pathways related to lymphocyte activation and differentiation with aging (Supplementary Fig. 2a, b). Gene Set Variation Analysis (GSVA) of each cell type showed that during the aging process, DNA-repair-related pathways such as sensing of DNA double-strand breaks were downregulated, while angiogenesis-related pathways, including integrin biosynthetic process and matrix metalloproteinases, were upregulated in all cell types (Supplementary Fig. 2c). Senescence-associated secretory phenotype (SASP) is a series of bioactive molecules produced by senescent cells which may promote tumor metastatic[1,4]. Our data showed the abundance of SASP genes increased with aging (Fig. 1h), and the senescence-associated β-galactosidase (SA-β-Gal) staining, a classical marker of cellular senescence, was also increased in all immune cells and neutrophil subset (Fig. 1i). In addition, we performed a comprehensive comparative analysis between aging DEGs and melanoma-related genes using the DisGeNET database. We found that aging mice had a higher abundance of melanoma-related genes compared to young mice, suggesting that aging might upregulate the expression of genes that promote tumor progression (Supplementary Fig. 2d). Furthermore, the score of cancer-related pathway gene sets in AC mice was higher than the YC in B cells and T cells (Supplementary Fig. 2e).

Collectively, we established an integral profile of aged lung tissue-resident immune cells and found that aging led to a pro-inflammation and pro-angiogenic phenotype with the recruitment and activation of neutrophils.

Aging alters the function and differentiation of MOMøDC and T cell

We then focused on two cell clusters whose proportional changes might not be readily apparent but played crucial roles in tumor

https://doi.org/10.1038/s41467-024-55164-3

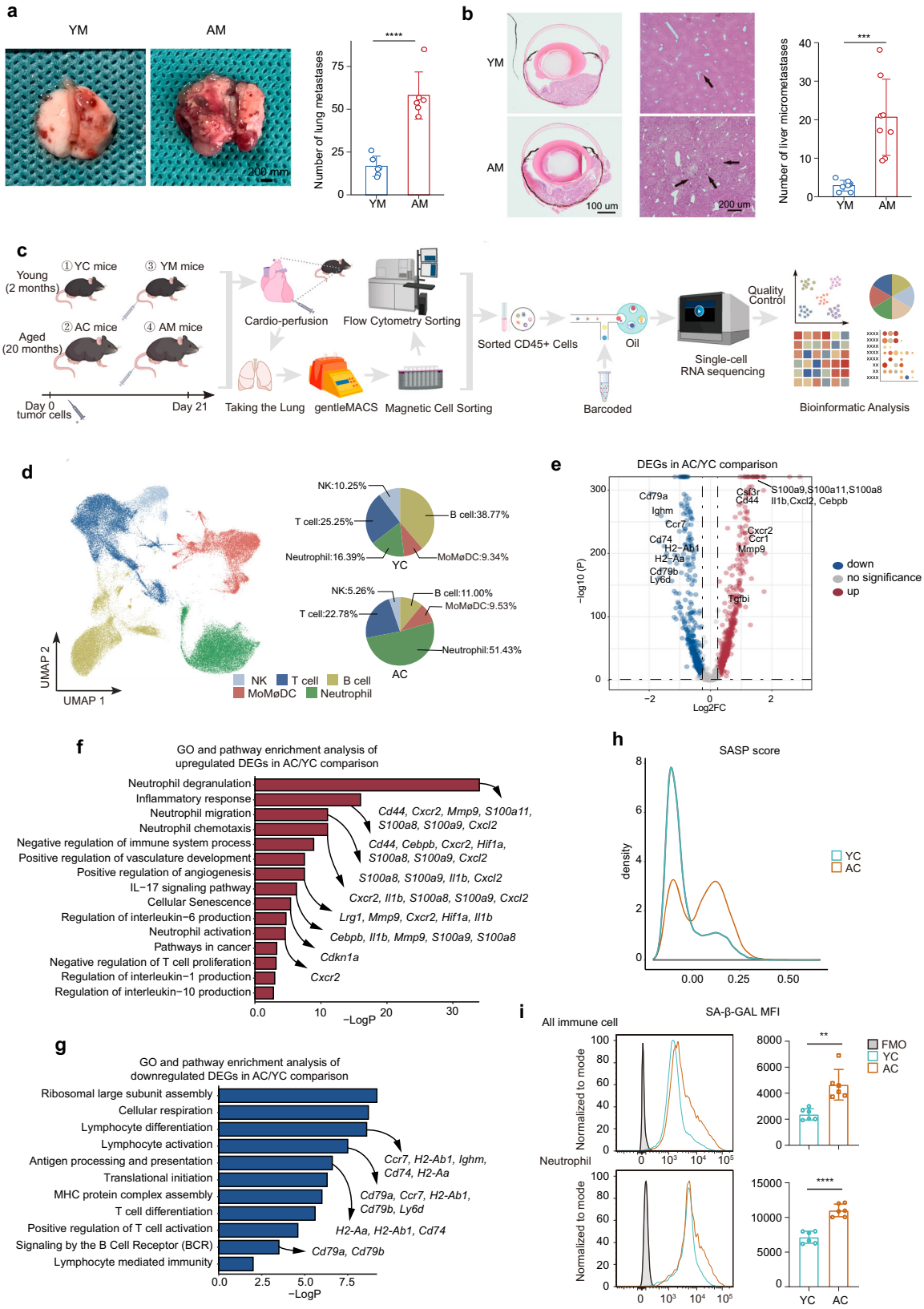

metastasis. MOMøDCs were found to drive cancer metastasis via immunosuppression[14] and angiogenesis[15]. Therefore, we further re-clustered MOMøDC into macrophages, monocytes, type 1 conventional dendritic cells (cDC1), type 2 conventional dendritic cells (cDC2), plasmacytoid dendritic cells (pDC), and mature dendritic cells enriched in immunoregulatory molecules (mregDC)[16] (Fig. 2a and Supplementary Fig. 3a, b). The proportion of each cell subset did not significantly differ between the young and aged control groups (Supplementary Fig. 3c). Analysis of DEGs showed that aging primarily affected dendritic cells, with a notable downregulated DEGs in mregDC and pDC (Supplementary Fig. 3d). Among the upregulated genes, pro-inflammatory genes, such as *Wfdc17, S100a8, S100a9*, and *Hsp90aa1*,

Fig. 1 | Study design and scRNA-seq analysis of aged lung immune microenvironment. a Representative images and quantitative results of lung metastases in young and aged mice. Each mouse was injected with 5×10^5 B16F10 cells via the tail vein. Each group contains six mice. Young mice are 2 months old, aged mice are 20 months old. Data expressed as mean ± SD. $P = 5.0E{-}05$. Significance was determined using unpaired two-tailed Student's t test. $^{****}P < 0.0001$. YM young model, AM aged model. Scale bars: 200 mm. **b** Representative images and quantitative results of liver metastases (arrow) after intraocular tumor establishment in young and aged mice. Each mouse was injected with 2.5×10^5 B16F10 cells via subretina. Young mice are 2 months old, aged mice are 20 months old. Each group contains eight mice. Data expressed as mean ± SD. $P = 1.7E{-}04$. Significance was determined using an unpaired two-tailed Student's t test. $^{***}P < 0.001$. Scale bars: 100 um, 200 um. **c** Schematic of the experimental design for scRNA-seq. YM and AM groups were respectively injected with B16F10 cells via the tail vein at day 0, and then the lung immune cells of YC, AC, YM, and AM groups were sorted for scRNA-seq at day 21. YC young control, AC aged control. Each image was drawn by PaintTool SAI (version 1.2) and Adobe illustrator 2023 (version 27.0). **d** Uniform manifold approximation and projection (UMAP) plot showing the cluster of cell types, pie charts showing the percentages of the immune cells in AC and YC groups. MoMøDC macrophages, monocytes and dendritic cells, NK natural killer cells. **e** Volcano plot showing upregulated and downregulated DEGs of all immune cells (as a whole) between AC and YC mice. Significance was determined using "FindMarkers" functions of Seurat package with Wilcoxon Rank Sum test and adjusted by Bonferroni correction. Representative GO terms and KEGG pathways enriched in upregulated DEGs (**f**) and downregulated DEGs (**g**) of all immune cells (as a whole) in the AC/YC comparison. Significance was calculated based on the accumulative hypergeometric distribution by Metascape webtool. **h** Kernel density estimation plot showing the shift of senescence-associated secretory phenotype (SASP) gene set score with age in total immune cells from mouse lung, calculated based on gene expression. The x-axis shows the range of scores, the y-axis indicates the calculated density, representing the likelihood of data falling within each range on the x-axis SASP: Senescence-associated secretory phenotype. **i** MFI of SA-β-Gal in all immune cells and neutrophils in lungs from YC/AC groups, which were measured by flow cytometry, calculated on CD45+ cells or CD45+CD11B+LY6G+ cells. Each group contains six mice. Data expressed as MFI of SA-β-Gal (mean ± SD). All immune cell ($P = 1.2E{-}03$), neutrophil ($P = 2.0E{-}05$). Significance was determined using unpaired two-tailed Student's t test. SA-β-Gal senescence-associated β-galactosidase, MFI mean fluorescence intensity. $^{****}P < 0.0001$, $^{**}P < 0.01$. Source data are provided as a Source Data file.

were commonly observed across various subtypes (Supplementary Fig. 3e). The GO and pathway enrichment analysis indicated that IL-17A-related pathways were upregulated in all subsets of myeloid cells in AC mice; angiogenesis-related pathways were enriched in monocytes and pDC, cell death- and cellular senescence- related pathways only in dendritic cells (Fig. 2b). The score of inflammation-related pathway was significantly increased in various subtypes during aging (Supplementary Figs. 3f and 4a). Furthermore, downregulated pathways were primarily found in dendritic cells and related to adaptive immunity, implying their decreased functions in modulating B cells and T cells. (Supplementary Fig. 4b). As monocytes can differentiate into both macrophages and dendritic cells, we investigated the differentiation trajectory of MOMøDC. Interestingly, the aging process affected the differentiation of mregDC, a type of dendritic cell with immunoregulation abilities found in various cancer types[17]. Along the pseudo-time course, MOMøDC cells exhibited two distinct states: state 1 and state 4 (Supplementary Fig. 4c). MregDCs in YC mice exclusively differentiated into state 4, while a substantial proportion in AC differentiated towards state 1 (Supplementary Fig. 4d). A comparison between these two states showed that mregDCs in state 1 exhibited an immunosuppressive state, with lower expression level of *Il12b* and CLEC7A (Dectin-1) signaling pathway components (Supplementary Fig. 4e, f), both of which are involved in anti-tumor immunity[17,18]. In addition, pathways related to immune activation, such as downstream TCR signaling and the positive regulation of T cell activation, were also downregulated in cells of state 1 (Supplementary Fig. 4f). Thus, aging induces a combination of pro-inflammatory and immunosuppressive phenotypes in MOMøDC.

Tumor-infiltrating T cells play a dual role in tumor metastasis, such as regulatory T cells (Treg) being tumor-promotive and CD8+ T cells being tumor-suppressive. This prompted us to make a more detailed examination of T cells. We classified T cells into five subtypes (Fig. 2c and Supplementary Fig. 5a, b): CD4+ T cells, CD8+ T cells, natural killer T cells (NKT), gamma delta T cells (γδT), and proliferative T cells. The AC mice had a reduced proportion of CD4+ T and proliferative T cells, an increased proportion of CD8+ T cells, γδT cells, and NKT cells (Fig. 2c). Given that a reduced CD4+/CD8+ T cell ratio is indicative of an immunosenescent state[19], we further substantiated this observation through flow cytometry analysis (Fig. 2d). Considering the pivotal role of lymph nodes and spleens as secondary lymphoid organs in mediating systemic immune responses to tumors[20], we extended our validation efforts to include these anatomical sites (Supplementary Fig. 5c). The GO and pathway analyses for each T cell subtype revealed that inflammation-associated pathways were upregulated in all subtypes, with the IL-17 signaling pathway showing the highest levels in γδT cells and inflammatory response pathways being most prominent in NKT cells, implying the involvement of T cells in aging-related inflammation (Fig. 2e). The pathways in cancer and the PD-1 related pathway were enhanced in most subtypes, whereas adaptive immune response related pathways were downregulated in proliferative T cells and CD8+ T cells, again pointing out the potential connection between aged T cells and cancer development (Fig. 2e and Supplementary Fig. 5d). Next, we used SCENIC package to predict the transcription factor regulatory network underlying aging to determine how the complex transcription regulation network is modulated by aging. By comparing the relative regulon activity of all cells from AC and YC mice, we obtained the top 10 age-dependent upregulated and downregulated transcription factors. Among them, Rora, a pivotal regulator of IL-17, showed the highest increase in transcriptional activity in AC mice compared to YC (Fig. 2f). Rorc, another transcription factor that regulates the IL-17 family members also showed higher activity (Fig. 2f). And these transcription factors were more closely associated with DEGs in γδT cells (Supplementary Fig. 5e). To determine the T cell subtypes in which these transcription factors were active, we conducted a regulon specificity score analysis across different cell subtypes in both YC and AC mice. In AC mice, the regulon specificity score of Rora and Rorc regulons in γδT cells were higher compared to any other subsets, and their activity levels were also much higher than those in YC mice (Fig. 2g and Supplementary Fig. 5f, g). Further, among all T cell subpopulations, IL-17A showed the highest expression level in γδT cells based on scRNA-seq data (Fig. 2h). γδ17 cells have been reported to exert pro-tumorigenic effects[21], combined with the result showing the increased γδ17 population in AC mice (Fig. 2c), we speculated that aging-enhanced tumor metastasis may be related with expansion of γδ17 cells.

Previous studies have reported that IL-17 can recruit neutrophils[22], which are able to suppress CD8+ T cell-mediated tumor killing[23]. Therefore, we speculated that the aging process may contribute to tumor metastasis through mechanisms involving the upregulation of γδ17 cells, recruitment of neutrophils, and suppression of CD8+ T cells. We used the CellphoneDB and CellChat packages to analyze intercellular communication including secreted signaling analysis and extracellular matrix-related signaling analysis. The results supported our hypothesis. The secreted signaling analysis from γδT to neutrophils was only seen in AC mice and the extracellular matrix-related signaling analysis from neutrophils to CD8+ T cells was much stronger in AC mice than in YC mice (Supplementary Fig. 6a, b). We then examined the top three enhanced ligand-receptor pairs between γδT|

https://doi.org/10.1038/s41467-024-55164-3

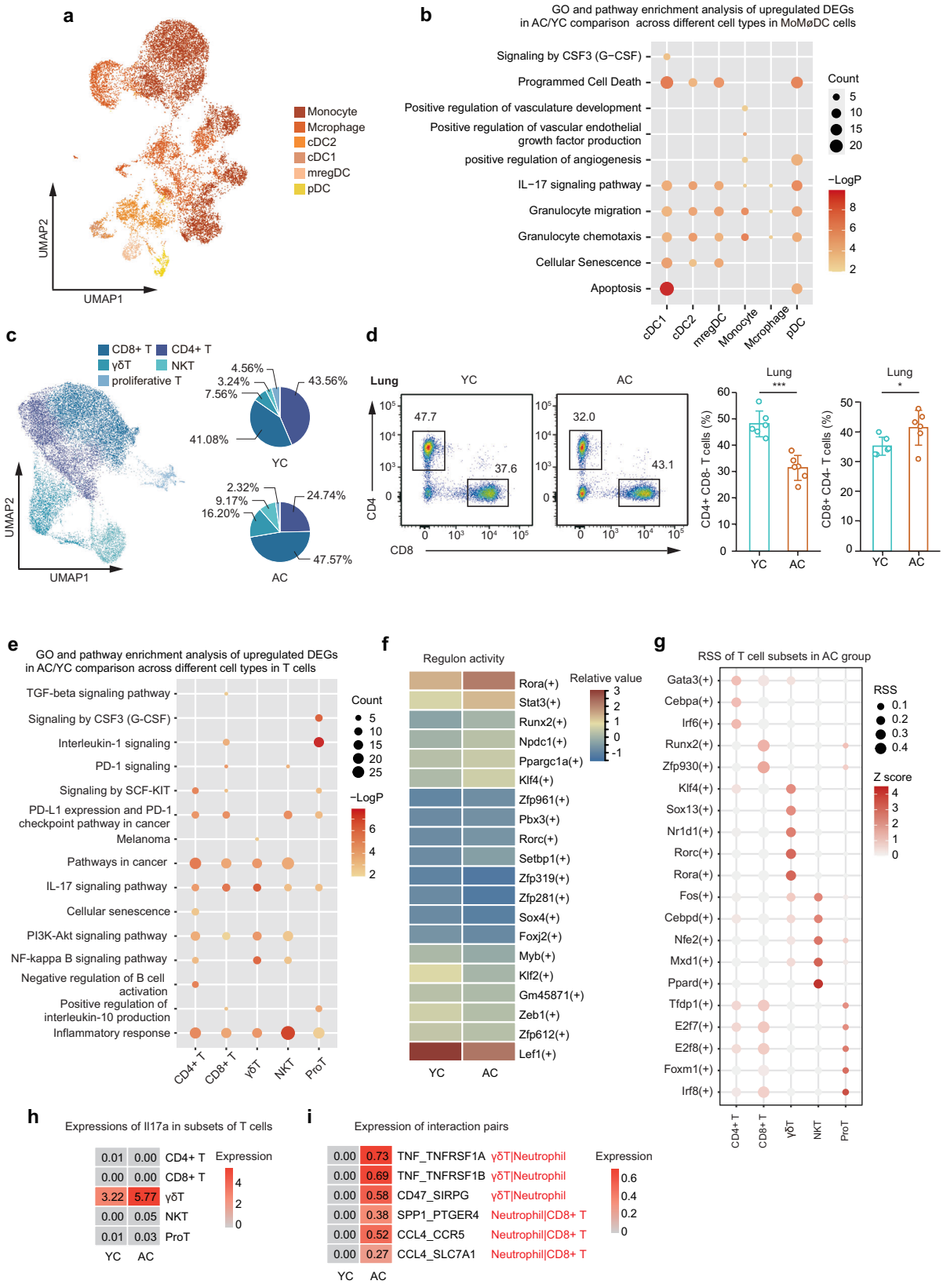

neutrophils and neutrophils|CD8+ T cells during the aging process (Fig. 2i). TNF-TNFRSF1A is required for IL-17-induced neutrophil infiltration[24]. CD47-SIRPG[25] and CCL4-CCR5[26] have been shown to contribute to tumor progression. The similar phenomena were observed in the modeled mice. T cells from YM mice showed increased relative regulon activity of Tcf7 and Lef1, indicating enhanced stemness, and T cells from AM mice exhibited higher relative regulon activity of Rorc (Supplementary Fig. 6c). Interestingly, Rorc and Rora emerged as top5 transcription factors in γδT cells of YM mice (Supplementary Fig. 6d). In AM mice, Rorc remained among the top5 transcription factors, and Hif, an oncogenic transcription factor, also displayed a high regulon specificity score (Supplementary Fig. 6e). In

Fig. 2 | scRNA-seq reveals the changes in aged myeloid and T cell subsets. **a** UMAP plot of myeloid cell subsets. cDC1 type 1 conventional dendritic cells, cDC2 type 2 conventional dendritic cells, mregDC mature dendritic cells enriched in immunoregulatory molecules, pDC plasmacytoid dendritic cells. **b** Dot plot showing representative GO terms and KEGG pathways enriched in upregulated DEGs of myeloid cell subsets in the AC/YC comparison. Significance was calculated based on the accumulative hypergeometric distribution by Metascape webtool. **c** UMAP plot of T cell subsets and Pie charts showing the percentages of the T cell subsets in AC and YC groups. NKT natural killer T cells, γδT gamma delta T cells. **d** Proportions of lung CD4+ and CD8+ T cells were measured by flow cytometry, gated on CD45+CD3+ cells. Each group contains six mice. Data expressed as % of CD4+ T cells or CD8+ T cells (mean ± SD). CD4+ ($P = 1.3E{-}04$), CD8+ ($P = 0.04$). Significance was determined using unpaired two-tailed Student's *t* test. $^{*}P < 0.05$, $^{***}P < 0.001$. **e** Dot plot showing representative GO terms and KEGG pathways enriched in upregulated DEGs of T cell subsets in the AC/YC comparison. Significance was calculated based on the accumulative hypergeometric distribution by Metascape webtool. **f** Heatmap exhibiting the top 10 active transcription factors of AC and YC groups, color key from blue to red indicates expression levels from low to high. **g** Dot plot showing top 5 regulon specificity score across T cell subsets in AC group. **h** Heatmap showing the average Il-17a expression levels across T cell subsets between AC and YC groups. **i** Cell-cell communication was analyzed by cellphoneDB, obtaining the expression level of interaction pairs among cell subtypes between AC and YC groups. Heatmap showing the expression of top three interaction pairs: TNF_TNFRSF1A, TNF_TNFRSF1B and CD47_SIRPG between γδT cells and neutrophils; SPP1_PTGER4, CCL4_CCR5 and CCL4_SLC7A1 between neutrophils and CD8+ T cells. Source data are provided as a Source Data file.

AM mice, the secreted signaling analysis from γδT to neutrophils was more visible and the extracellular matrix-related signaling analysis from neutrophils to CD8+ T cells was much stronger than in YM mice (Supplementary Fig. 6f, g). IL-17A continued to show the highest expression in γδT cells (Supplementary Fig. 6h). Additionally, the tumor-promoting pairs CCL3-CCR5[27] and PDCD1-CD274[28], were upregulated (top 3) with aging in γδT|neutrophil and neutrophil|CD8+ T cells, respectively (Supplementary Fig. 6i). Taken together, these findings indicate the γδ17, neutrophils, and CD8+ T cells may be involved in the increased metastatic propensity induced by aging.

Aging facilitates the expansion of γδ17 and the recruitment of neutrophils

Following the identification of deviations in γδ17, neutrophils, and CD8+ T cells in aged mice, we decided to analyze whether these alterations indeed hold substantial importance in age-induced cancer metastasis. We first assessed the proportions of these cells in YC, YM, AC and AM mice. In the lungs, the proportion of γδT cells significantly increased with age, and this difference was further exacerbated in tumor-bearing mice, indicated by scRNA-seq and further verified by flow cytometry (Supplementary Fig. 7a and Fig. 3a). This was consistent with the quantitative data (Fig. 3b). We also analyzed the cells from lymph nodes and spleens to explore the correlations between local and systemic responses. The results from lymph nodes showed a pattern like that observed in the lungs (Supplementary Fig. 7b, c), spleens displayed a moderate different pattern, with a lower ratio of γδT cells in aged mice (Supplementary Fig. 7d, e). To further investigate the factors contributing to that increase in lungs, we analyzed the DEGs of γδT between the four pair-wise comparisons (Fig. 3c). Two DEGs, *Cd69* and *S1pr1* aroused our special attentions. CD69 is an early immune system activation marker[29], which functions as a negative regulator of S1pr1[30]. S1pr1 is an egress receptor required for lymphocyte trafficking[31]. γδT cells are a kind of tissue-resident cell, primarily self-renewing and partially migrating from peripheral immune organs[32]. We observed a higher expression of CD69 in γδT cells of aged mice in the lungs, lymph nodes and spleens (Fig. 3d and Supplementary Fig. 7f, g). Correspondingly, the expression of S1pr1 was downregulated in lung tissue-resident γδT cells (Fig. 3e), upregulated in lymph nodes and it did not exhibit statistical significant in spleens during the aging process (Supplementary Fig. 7h, i). This differential expression of S1pr1 could retain lung-resident γδT cells and indicate the migration of γδT cells from lymph nodes to the lungs. GO and pathway analyses of γδT cells indicated that both aging and tumor burden increased IL-17 signaling pathway in these cells (Supplementary Fig. 7j). Interestingly, neutrophil degranulation pathway and neutrophil chemotaxis pathway were enhanced in the presence of tumor burden and aging process, which may indicate the increased interaction between γδT cells and neutrophils. Data from scRNA-seq and flow cytometry further supported the upregulation of the IL-17 expression in aged groups, and tumor burden further increased IL-17 expression in ages mice, with no discernible difference observed in young mice (Fig. 3f, g). The alteration of γδ17 in lymph nodes and spleens were consistent with that observed in the lungs (Supplementary Figs. 7k and 8a). It has been reported that γδT cells have a dual role towards tumor, with γδ17 cells promoting tumor growth and IFN-γ-producing γδT cells (γδ1) inhibiting[33]. The proportion of γδ1 showed no significant difference among the four groups in all examined tissues (Supplementary Fig. 8b–d). We further examined the expression levels of S1pr1 in γδ17 cells across the four groups and found that the changes in S1pr1 expression followed the same trend as observed in the overall γδT cell population (Supplementary Fig. 8e). These results suggest that aging could increase the proportion of γδ17 cells possibly via differential expression of S1pr1 and the presence of a tumor seems to further enhance this difference.

Given that IL-17 can recruit neutrophils, we subsequently examined changes in the neutrophil ratio during aging. Single-cell and flow cytometry data consistently revealed that aging increases lung-resident neutrophils (Supplementary Fig. 8f and Fig. 3h, i). Additionally, flow cytometry analysis confirmed that tumors exhibit a synergistic effect with aging in this context (Fig. 3h, i). On the other hand, in lymph nodes and spleens, aging increases the proportion of neutrophils in tumor-bearing mice (Supplementary Fig. 8g, h). Bone marrow is an important storage pool for neutrophils and serves as a source of peripheral neutrophils[34]. Therefore, we also collected cells from bone marrow, disclosing a similar pattern aligned with lungs (Supplementary Fig. 8i). Together, aging increased the proportion of neutrophils, and this increase was specifically more pronounced in tumor-bearing aged mice.

γδ17 skew neutrophils toward a more pro-tumoral phenotype in aging

Given the results showing neutrophil expansion and increased IL-17 pathways, we investigated their connections to explore the possible mechanisms of immune remodeling during aging. It is known that CXCR2 is a chemokine receptor primarily expressed in neutrophils[35]. It responds to IL-17A and mediates neutrophil migration towards tumor sites[36]. Thus, we examined the CXCR2 levels expressed in neutrophils of bone marrow and found increased CXCR2 levels in the aged groups, regardless of the presence of tumors, indicating a stronger mobilization signal from the bone marrow to the peripheral tissues with aging (Fig. 4a, b).

Next, we further investigated the alterations in neutrophil function caused by aging. Through GSVA analysis of neutrophils, we discovered that the predominant pathways increased by both tumor bearing and aging are among the kit-related pathways (Fig. 4c). C-kit is a hallmark of premature neutrophils associated with tumor invasion[37]. We observed its significant increase in the lungs during aging, whether with tumor bearing (Fig. 4d). Additionally, the expression of c-kit exhibited an increase in bone marrow neutrophils from aged mice, with a statistically significant difference between YM and AM mice

https://doi.org/10.1038/s41467-024-55164-3

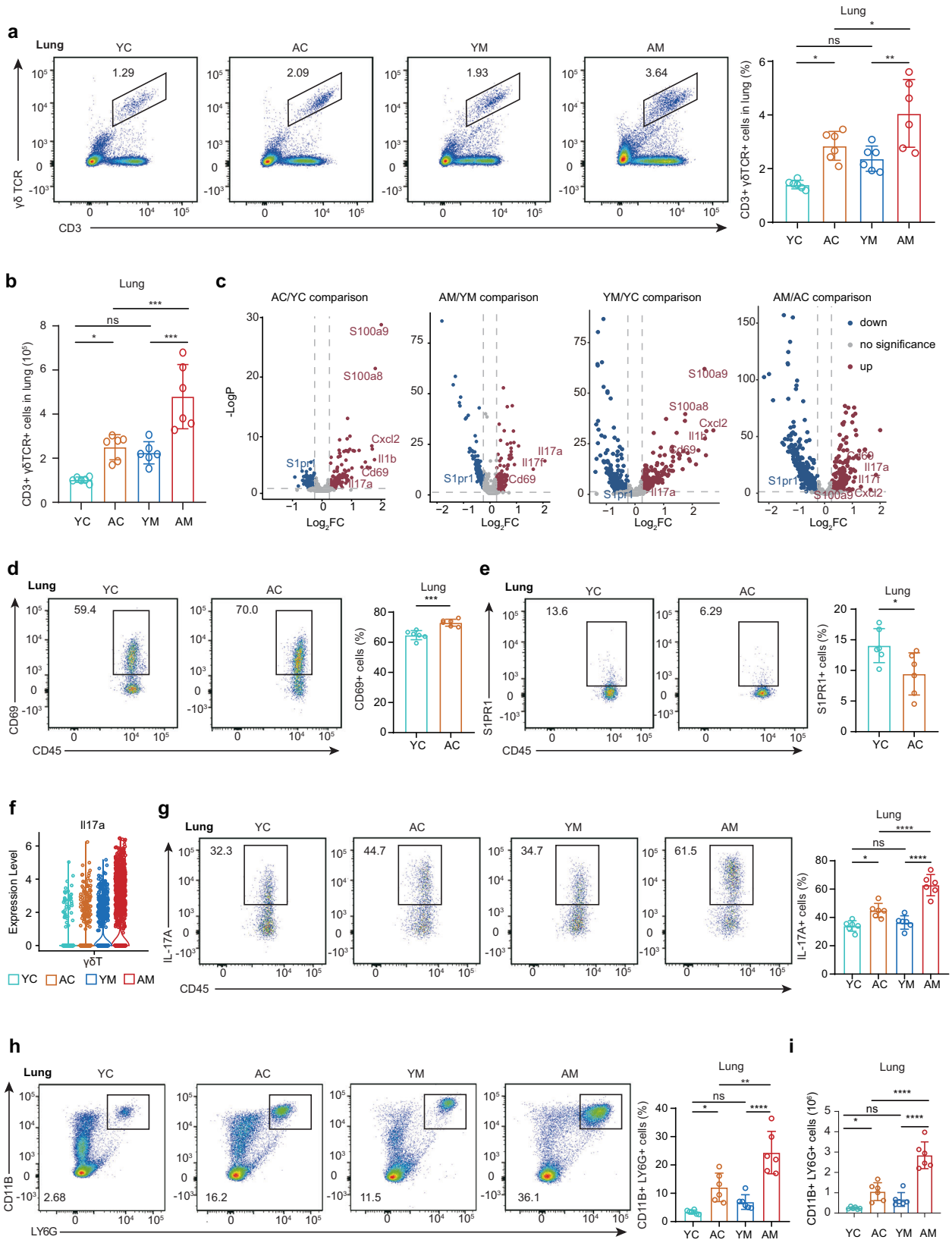

(Supplementary Fig. 9a). From GO and pathway analyses, we found that neutrophils in aged mice demonstrated reduced overall metabolic activity (Supplementary Fig. 9b), relatively higher level of Rho GTPase-related signaling and reactive oxygen species process-related signaling (Fig. 4e). Both Rho GTPase and reactive oxygen species have tumor-promoting effects[38,39], and their related pathways are more significantly elevated in the AM mice. Importantly, in tumor bearing mice, we found that aging promoted neutrophil extracellular traps formation (Fig. 4e). Neutrophil extracellular traps are extracellular structures released by active neutrophils and are linked to promoting inflammation for tumor progression[40]. These changes together pointed to active neutrophils which had been shown to promote

Fig. 3 | Aging facilitates the recruitment of tissue-resident γδ17 and neutrophils. a Proportions of lung γδT cells were measured by flow cytometry, gated on CD45+ cells. Each group contains six mice. Data expressed as % of γδT cells (mean ± SD). YC-AC ($P = 0.01$), AC-AM ($P = 0.04$), YM-AM ($P = 3.5E{-}03$). Significance was determined using one-way ANOVA. $^{*}P < 0.05$, $^{**}P < 0.01$, $^{***}P < 0.001$, ns no significance, $P > 0.05$. **b** Quantity of γδT cells in per 0.1 g lung. Each group contains six mice. Data expressed as number of γδT cells (mean ± SD). YC-AC ($P = 0.02$), AC-AM ($P = 6.0E{-}04$), YM-AM ($P = 2.0E{-}04$). Significance was determined using one-way ANOVA. $^{*}P < 0.05$, $^{**}P < 0.01$, $^{***}P < 0.001$, ns no significance, $P > 0.05$. **c** Volcano plot showing DEGs in AC/YC, AM/YM, YM/YC, and AM/AC comparison. Significance was determined using the "FindMarkers" functions of the Seurat package with the Wilcoxon Rank Sum test and adjusted by Bonferroni correction. Proportions of lung CD69 + γδT (**d**) and S1PR1 + γδT (**e**) cells from AC and YC mice were measured by flow cytometry, gated on CD45+CD3+γδTCR+ cells. Each group contains six mice. Data expressed as % of CD69 + γδT or S1PR1 + γδT cells (mean ± SD). $P = 3.4E{-}04$ (**d**); $P = 0.03$ (**e**). Significance was determined using an unpaired two-tailed Student's *t* test. $^{*}P < 0.05$. **f** Violin plot showing average expression levels of IL-17A in γδT cells in each group, based on the scRNA-seq data. **g** Proportions of lung IL-17A + γδT cells were measured by flow cytometry, gated on CD45+CD3+γδTCR+ cells. Each group contains six mice. Data expressed as % of γδ17 cells (mean ± SD). YC-AC ($P = 0.01$), AC-AM ($P = 7.1E{-}05$), YM-AM ($P = 2.8E{-}07$). Significance was determined using one-way ANOVA. $^{*}P < 0.05$, $^{****}P < 0.0001$, ns $P > 0.05$. **h** Proportions of lung neutrophils were measured by flow cytometry, gated on CD45+ cells. Each group contains six mice. Data expressed as % of neutrophils (mean ± SD). YC-AC ($P = 0.02$), AC-AM ($P = 1.1E{-}03$), YM-AM ($P = 1.6E{-}05$). Significance was determined using one-way ANOVA. $^{*}P < 0.05$, $^{**}P < 0.01$, $^{****}P < 0.0001$, ns $P > 0.05$. **i** Quantity of neutrophils in per 0.1 g lung. Each group contains six mice. Data expressed as number of neutrophils (mean ± SD). YC-AC ($P = 0.02$), AC-AM ($P = 3.5E{-}06$), YM-AM ($P = 1.7E{-}07$). Significance was determined using one-way ANOVA. $^{*}P < 0.05$, $^{****}P < 0.0001$, ns $P > 0.05$. Source data are provided as a Source Data file.

metastasis, characterized by higher expression level of CXCR4 and lower CD62L[41,42]. Using flow cytometry, we confirmed that aging elevated CXCR4 expression, with a more pronounced effect in model mice, and reduced CD62L expression in both AC and AM lung tissues (Fig. 4f and Supplementary Fig. 9c). A similar trend was also observed in the bone marrow (Supplementary Fig. 9d, e). Next, we investigated the potential molecular factors behind increased neutrophil activity in aging mice. Toll-like receptors and CD54 are known to boost neutrophil activity[43]. We found aging did not alter TLR2 expression in lung and bone marrow neutrophils (Supplementary Fig. 9f, g), but it increased TLR4 expression in the lung (Supplementary Fig. 9h) with no changes in the bone marrow (Supplementary Fig. 9j). Aging also elevated CD54 expression in lung neutrophils of AM (Supplementary Fig. 10a), not in the bone marrow (Supplementary Fig. 10b). These findings may partly explain the increased neutrophil activity observed in aging mice.

To determine whether these neutrophil phenotype changes were associated with γδ17 cells, we depleted γδT cells in mice using an anti-γδTCR antibody[44] (Supplementary Fig. 10c). The number of pulmonary metastatic foci decreased significantly in AM mice, but not in YM mice (Fig. 4g, h and Supplementary Fig. 10d, e). Whereas γδT-depletion decreased the proportion and number of total neutrophils in both YM and AM mice, it only reversed the increased proportion of immature neutrophils, elevated CXCR4 expression, and decreased CD62L expression in AM mice (Fig. 4i, j and Supplementary Fig. 10f, g). In conclusion, aging increased the abundance of γδ17 cells, which can recruit neutrophils and potentially induce their transition to a pro-tumorigenic phenotype.

Neutrophils inhibit the proliferation of CD8+ T cell through Arg2

As shown in Fig. 4e, AM mice exhibited increased negative regulation of the T-cell proliferation pathway compared with YM mice. Since CD8+ T cells play a vital role in anti-tumor immunity, we proceeded to investigate the impact of neutrophils on CD8+ T cells. From these GSVA analysis of neutrophils in the YC, YM, AC and AM mice, we observed that several arginine-related pathways were altered by aging, such as arginase activity, arginine metabolic and catabolic processes (Fig. 5a). Arginase catalyzes the breakdown of arginine, thereby inhibiting the proliferation of activated T cells[45]. Our further scRNA-seq analysis showed that *arginase 2* (*Arg2*) was expressed at a higher level in the neutrophils of AM than YM mice (Fig. 5b). Flow cytometry also revealed a higher expression of Arg2 in neutrophils from the lungs and bone marrow of tumor-bearing mice (Fig. 5c, d). This difference was not observed in tumor-free mice (Supplementary Fig. 10h–j).

To further explore the impact of neutrophil-derived Arg2 on CD8+ T cells, we first examined the levels of Arg2 in both serum and the supernatant of bone marrow-derived neutrophil cultures. The concentration of Arg2 in the serum and neutrophil culture medium was found to be increased in both aged groups (Fig. 5e, f). Subsequently, we designed an in vitro co-culture experiment. CD8+ T cells isolated from the spleen of YC mice were cultured with bone marrow neutrophils from YM and AM mice, with or without BEC hydrochloride, which functions as an inhibitor of Arg2 (Fig. 5g). We found that neutrophils from AM mice significantly suppressed the proliferation CD8+ T cells, and this inhibition was reversed by the additional BEC hydrochloride (Fig. 5h). Since PD-1 is commonly utilized by cancer cells to evade immune detection and can inhibit T cell proliferation, we also assessed the expression levels of PD-1 in CD8+ T cells. CD8+ T cells co-cultured with neutrophils from AM mice exhibited a significantly higher ratio of exhausted PD-1+ CD8+ T cells (Fig. 5i).

Neutrophils from the aged male mice suppress the stemness of CD8+ T cell

Considering the pro-tumor role of neutrophils within the aging microenvironment, we used Ly6G-specific antibodies to deplete neutrophils[46]. Depleting neutrophils resulted in notable pulmonary metastatic foci decrease in AM mice, with no apparent impact in YM (Fig. 6a, b and Supplementary Fig. 11a, b). Furthermore, the percentage and number of tumor-infiltrating CD8+ T cells significantly increased in aged mice, but not in the young (Supplementary Fig. 11c, d). Similar results were observed in the lymph nodes (Supplementary Fig. 11e, f). Therefore, we focused on CD8+ T cells to dissect the detailed mechanism regarding how neutrophils modulated T cells during aging.

First, we examined age-related transcriptional alterations in CD8+ T cells. During aging, the proportion of naïve CD8+ T cells (Cd44-Cd62l+) decreased, and the percentage of terminally exhausted CD8+ T cells (Havcr2+Pdcd1+) increased (Supplementary Fig. 11g, h), indicating a gradual decline of CD8+ T cells functionality. A subset of DEGs results from AC/YC and AM/YM were similar: markers of exhaustion such like *Pdcd1*, *Tox* and *Tigit* were upregulated, while markers of stemness[47] such as *Tcf7*, *Ccr7*, and *Sell* were downregulated (Supplementary Fig. 11i). The number of overlap DEGs between AC/YC and AM/YM comparison was significant (Supplementary Fig. 11j). GSVA analysis revealed upregulation of the immunosuppression pathways in aged CD8+ T cells, along with downregulation of proliferation and cell killing-related pathways (Fig. 6c). All the aforementioned alterations pointed towards the loss of CD8+ T cells stemness during aging. We then contemplated whether the decrease of CD8+ T cell stemness could be attributed to neutrophils. Therefore, we proceeded with the neutrophil depletion strategy. It presented a noteworthy upregulation in the expression of TCF1 (encoded by *Tcf7*) and Ki67 (a biomarker for proliferation) within the CD8+ T cells at the tumor site in aged mice (Fig. 6d, e), suggesting an enhanced state of stemness. This difference was not observed in young mice (Supplementary Fig. 12a, b). Similar results regarding TCF1 were

https://doi.org/10.1038/s41467-024-55164-3

observed in lymph nodes (Supplementary Fig. 12c, d). The pattern of Ki67 expression showed similarity in spleens (Supplementary Fig. 12e, f). Intriguingly, in lymph nodes, neutrophil depletion lowered the ratio of Ki67+CD8+ T cells in young mice but did not alter it in aged animals (Supplementary Fig. 12g, h). After removing neutrophils from aged mice, the tumor-infiltrating CD8+ T cells exhibited a higher percentage of CD44-CD62L+ (naïve), CD44+CD62L+ (central memory), and a lower percentage of CD44+CD62L- (effector memory) phenotype (Fig. 6f and Supplementary Fig. 12i). Given that T cells differentiate from naïve to memory, progressing from central memory to effector memory, this transition signifies a shift towards a stem cell-like phenotype. In contrast, this shift was not statistically significant in young mice (Supplementary

Fig. 4 | γδ17 rendered neutrophils to present a more pro-tumoral phenotype in an aging state. Proportions of CXCR2+ cells in neutrophils in bone marrow from AC/YC groups (**a**) and AM/YM groups (**b**), measured by flow cytometry, gated on CD45+CD11B+LY6G+ cells. Each group contains six mice. Data expressed as % of CXCR2+ neutrophils (mean ± SD). $P = 4.8E{-}03$ (**a**); $P = 2.1E{-}05$ (**b**). Significance was determined using unpaired two-tailed Student's *t* test. $^{**}P < 0.01$, $^{****}P < 0.0001$. **c** Based on the scRNA-seq data from lung, heatmap showing representative KEGG pathways of neutrophils across AC, YC, AM and YM groups, calculated by GSVA packages. Color key from white to red indicates expression levels from low to high. **d** Proportions of lung c-Kit+ neutrophils were measured by flow cytometry, gated on CD45+CD11B+LY6G+ cells. Each group contains six mice. Data expressed as % of c-Kit+ neutrophils (mean ± SD). YC-AC ($P = 0.01$), YM-AM ($P = 1.0E{-}04$). Significance was determined using one-way ANOVA. $^{*}P < 0.05$, $^{***}P < 0.001$, ns $P > 0.05$. **e** Dot plot showing representative GO terms and KEGG pathways enriched in upregulated DEGs of neutrophils in the AC/YC and AM/YM comparison. Significance was calculated based on the accumulative hypergeometric distribution by Metascape webtool. **f** MFI of CXCR4 in neutrophils of lung from AM/YM/AC/YC groups, which were measured by flow cytometry, gated on CD45+CD11B+LY6G+ cells. FMO fluorescence minus one control. Each group contains six mice. Data expressed as MFI of CXCR4 (mean ± SD). YC-YM ($P = 8.4E{-}03$), AC-AM ($P = 1.1E{-}06$), YM-AM ($P = 3.5E{-}04$). Significance was determined using one-way ANOVA. $^{**}P < 0.01$, $^{***}P < 0.001$, $^{****}P < 0.0001$, ns $P > 0.05$. Representative images and quantitative results of lung metastases in aged (**g**) and young (**h**) mice with anti-γδTCR or isotype (control) treated. Each group contains six mice. Data expressed as number of metastases (mean + SD). $P = 0.01$ (**g**); $P = 0.7$ (**h**). Significance was determined using unpaired two-tailed Student's *t* test. $^{*}P < 0.05$, ns $P > 0.05$. Proportions and quantity of neutrophils (**i**) and c-Kit+ neutrophils (**j**) were measured by flow cytometry, gated on CD45+ cells or CD45+CD11B+LY6G+ cells. Each group contains six mice. Data expressed as % or number of neutrophils, c-Kit+ neutrophils (mean ± SD). Neutrophils-ratio: AM ($P = 2.3E{-}05$), YM ($P = 6.5E{-}03$); Neutrophils-number: AM ($P = 1.4E{-}04$), YM ($P = 0.03$). c-kit+ neutrophils-ratio: AM ($P = 6.74E{-}03$), YM ($P = 0.93$); c-kit+ neutrophils-number: AM ($P = 1.8E{-}03$), YM ($P = 0.08$). Significance was determined using unpaired two-tailed Student's *t* test. $^{*}P < 0.05$, $^{**}P < 0.01$, $^{***}P < 0.001$, $^{****}P < 0.0001$, ns $P > 0.05$. Source data are provided as a Source Data file.

Fig. 12j). A similar trend was observed in spleens (Supplementary Fig. 13a, b). However, the CD8+ T cells stemness of lymph nodes showed a decrease in young mice after neutrophil depletion (Supplementary Fig. 13c, d). Together with the results of Ki67, it may suggest an age-based effect of neutrophils on CD8+ T cells. In addition, neutrophil depletion diminished the ratio of Tim3+PD-1+CD8+ T cells (terminally exhausted) in lungs from AM mice, not in YM mice (Fig. 6g and Supplementary Fig. 13e). In the peripheral lymphoid organs, the proportion of Tim3+PD-1+CD8+ T cells appeared to be unaffected by neutrophils; but the PD-1 single-positive CD8+ T cells possessed the same pattern (Supplementary Fig. 14a–d). The cytotoxicity of CD8+ T cells against tumor cells was characterized by the secretion of IFN-γ, TNF, and GZMB. We discovered that the percentage of IFN-γ+TNF+CD8+ T cells and GZMB+CD107a+CD8+ T cells (CD107a is a marker of active degranulation[48]) were both increased in the tumor microenvironment of aged mice after neutrophil depletion (Fig. 6h, i), but not in young mice (Supplementary Fig. 14e, f). The same age-based alteration of IFN-γ+TNF + double-positive CD8+ T cells could also be observed in lymph nodes (Supplementary 14g, h). All these results highlight that neutrophil depletion could rescue the stemness of CD8+ T cells in aging mice.

Stem cell-like CD8+ T cells, annotated as PD1+TCF1+Tim3-CD8+ T cells, are a recently identified cell population responsible for immune checkpoint blockade[48]. In our study, we further clustered the CD8+ T cells[48] (Supplementary Fig. 15a) and observed a decrease in stem cell-like CD8+ T cells ratio in aged mice (Fig. 6j). This decrease was reversed by neutrophil depletion (Fig. 6k and Supplementary Fig. 15b). Once again, our findings revealed that neutrophil depletion does not significantly influence the stem cell-like CD8+ T cells population at the tumor site of YM mice, and even decrease the stem cell-like CD8+ T cells ratio in spleens (Supplementary Fig. 15c–e). Subsequently, we seek to elucidate the possible mechanism through which neutrophils influence CD8+ T cell stemness. It is established that PD-L1 (a ligand of PD-1) expressed on neutrophils can facilitate tumor progression and induce CD8+ T cell exhaustion[49]. In our study, PD-L1 expression on neutrophils was elevated in AM mice compared to YM mice (Supplementary Fig. 15f), and neutrophil depletion could decrease the exhaustion ratio of CD8+ T cells as found before. Additionally, we found that neutrophil depletion increased the ratio of CD4+ T cells without altering Treg cells in YM mice, while it decreased Treg cells without affecting CD4+ T cells in AM mice (Supplementary Fig. 15g, h). Neutrophils can promote Treg cell differentiation[50], which can cause CD8+ T cell exhaustion[51] in tumor. Overall, our findings suggest that lung neutrophils in aged male mice have a detrimental effect on the stemness of CD8+ T cells and promote the transition of CD8+ T cells towards an exhaustive phenotype. A comparable pattern was observed in peripheral immune organs. The depletion of neutrophils enhances the stemness of CD8+ T cells to inhibit tumor metastasis in aged male mice, potentially by regulating the PD-1/PD-L1 axis and Treg cells, while offering no advantages and could even cause adverse effects in young mice.

Procyanidin C1 reversed the tumor-promoting effect of aging

PCC1, a recently identified phytochemical senolytic agent, has been reported to effectively eliminate senescent cells induced by various stressors[52,53]. Given the results above indicating aging played a critical role, we therefore attempted to explore whether this senolytic agent could ameliorate age-related immune-suppression and subsequently inhibit tumor metastasis. We administered PCC1 to AM mice and an equivalent volume of solvent to the control group. Encouragingly, the application of PCC1 significantly reduced the number of lung tumor metastatic foci (Fig. 7a, b). To further understand the underlying mechanism, we assessed the proportions of key cells involved in the γδ17-Neutrophil-CD8 axis. Following the administration of PCC1, a noticeable reduction in the γδT and γδ17 ratio was observed in both the tumor microenvironment and the peripheral lymphatic organs (Fig. 7c, d and Supplementary Fig. 16a, b). The proportions of neutrophils and their CXCR4 expression at the tumor local site exhibited a similar reduction trend (Fig. 7e, f), and CD62L exhibited an increasing trend (Fig. 7g). Simultaneously, the proportion of CD8+ T cells, TCF1 expression of CD8+ T cells and ratio of stem cell-like CD8+ T cells were significantly increased following the administration of PCC1 (Supplementary Fig. 16c–e). SA-β-gal and P53 are classical markers of cellular senescence. We found that PCC1 administration decreases the expression of SA-β-gal and P53 in both γδT cells and neutrophils (Fig. 7h, i and Supplementary Fig. 16f, g). These results suggest that PCC1 could clear senescent γδT cells and neutrophils, consistent with our previous research showing that PCC1 can selectively clear senescent cells[52]. Additionally, PD-L1 expression on neutrophils was also downregulated (Supplementary Fig. 16h). These alterations may partially explain the inhibitory mechanisms of PCC1 on the γδ17-Neutrophil-CD8 axis, but further studies are needed as research on PCC1 is still in its early stages. In conclusion, our findings suggest that PCC1 can counteract the aging-induced changes in the γδ17-Neutrophil-CD8 axis, thereby effectively reducing tumor metastasis.

Discussion

Aging has gradually emerged as a research hotspot owing to global aging trends. Tumor metastasis is a life-threatening process, and the impact of aging regarding cancer is a topic of great interest and remains poorly understood. We found that aging promotes melanoma metastasis in male mice, which is consistent with the findings

https://doi.org/10.1038/s41467-024-55164-3

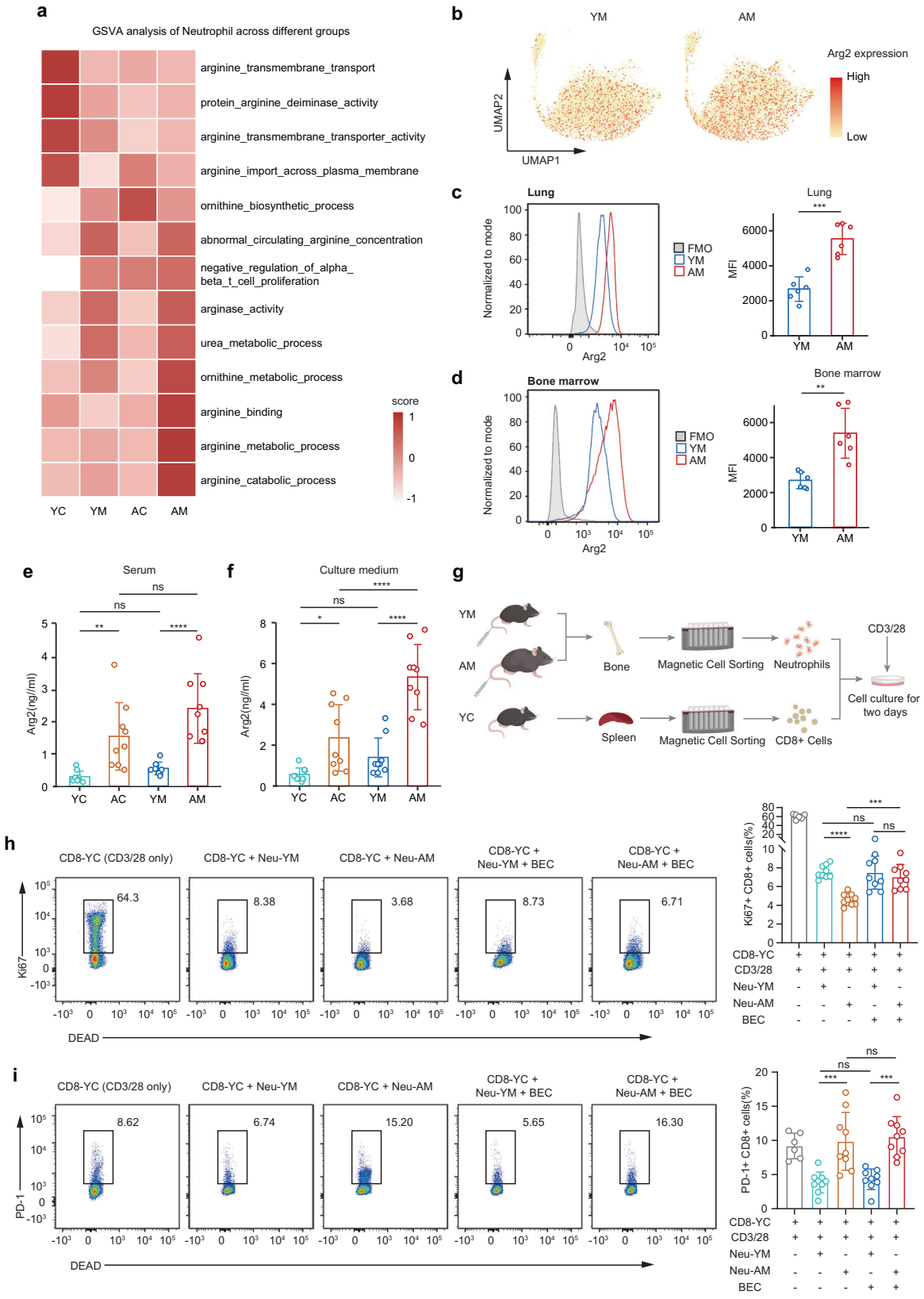

of previous studies[54–56]. These studies predominantly focused on elucidating the influence of aging on the extracellular matrix and its role in promoting tumor metastasis. Building on these findings, our study further explored the impact of aging on the immune microenvironment and its contribution to tumor metastasis. By applying scRNA-seq, a powerful tool to dissect the cell specific contribution, we identified the important role of neutrophils and γδT cells during aging and demonstrate that aging can impair the anti-tumor activity through the γδ17-Neutrophil-CD8 axis in male mice, subsequently promoting metastasis. Regarding the translational value, the senolytic agent PCC1 intervenes in this axis, effectively curtailing tumor metastasis.

Fig. 5 | Neutrophils inhibited the proliferation of CD8+ T cells through Arg2 in aged tumor-bearing mice. a Heatmap showing representative GO terms of neutrophils across AC, YC, AM and YM groups, calculated by GSVA packages. Color key from white to red indicates expression levels from low to high. **b** Feature plots showing the expression levels Arg2 in neutrophils between AM and YM groups based on scRNA-seq. Arg2 arginase 2. MFI of Arg2 in neutrophils of lung (**c**) and bone marrow (**d**) from AM/YM groups, which were measured by flow cytometry, gated on CD45+CD11B+LY6G+ cells. FMO fluorescence minus one control. Each group contains six mice. Data expressed as MFI of Arg2 (mean ± SD). $P = 1.0E{-}04$ (**c**), $P = 1.3E{-}03$ (**d**). Significance was determined using unpaired two-tailed Student's *t* test. $^{***}P < 0.001$. The expression of the Arg2 protein in serum (**e**) and supernatants from the neutrophil culture medium (**f**) was measured using enzyme-linked immunosorbent assay. Neutrophils were cultured 2 days for its supernatants collection. Each group contains nine mice. Data expressed as the concentration of Arg2 (mean ± SD). **e** YC-AC ($P = 7.7E{-}03$), YM-AM ($P = 7.0E{-}05$). **f** YC-AC ($P = 0.02$), AC-AM ($P = 9.1E{-}05$), YM-AM ($P = 8.4E{-}07$). Significance was determined using one-way ANOVA. $^{*}P < 0.05$, $^{**}P < 0.01$, $^{****}P < 0.0001$, ns $P > 0.05$. **g** The experimental workflow of neutrophils co-culture with CD8+ T cells. Each image was drawn by PaintTool SAI (version 1.2) and Adobe Illustrator 2023 (version 27.0). Proportions of Ki67+CD8+ T cells (**h**) and PD-1+CD8+ T cells (**i**) in the co-culture system were measured by flow cytometry, gated on CD45+CD8+ cells. BEC an Arg2 inhibitor, Neu neutrophil. Each group contains nine mice. Data expressed as % of Ki67+CD8+ or PD-1+CD8+ cells (mean ± SD). **h** Neu-YM vs. Neu-AM ($P = 6.1E{-}05$), Neu-AM vs. Neu-AM + BEC ($P = 9.6E{-}04$); **i** Neu-YM vs. Neu-AM ($P = 4.0E{-}04$), Neu-YM + BEC vs. Neu-AM + BEC ($P = 2.6E{-}04$). Significance was determined using one-way ANOVA. $^{***}P < 0.001$, $^{****}P < 0.0001$, ns $P > 0.05$. Source data are provided as a Source Data file.

Previous studies have provided a single-cell landscape atlas of all cells in aging lungs and found that aging can lead to the dysregulation of epigenetic control[57]. However, a detailed exploration of the immune microenvironment in these studies was lacking. In our study, we focus on the immune cell atlas of aged lungs, aiming to address this gap. Our findings also highlight a shift in the immune microenvironment towards the premetastatic niche during aging. The premetastatic niche is a favorable environment for metastasis to secondary organs induced by the primary tumor. In this study, we found that lung immunity presents a pro-angiogenic state and an inflammatory state during aging, characterized by the recruitment of neutrophils and the upregulation of inflammatory pathways. The expansion of NKT cells, which upregulate immune response pathways, may also contribute to this outcome. Analysis of B cells and NK cells also demonstrates that aging leads to an immunosuppressive state. Furthermore, cancer pathways and the enrichment score of melanoma-related gene sets are also enhanced during aging, which further predisposes aged male mice to cancer. MregDCs are a recently characterized cell type, and no relevant studies to date have investigated the effects of aging on mregDCs. Our findings suggest that aging alters the differentiation trajectory of mregDCs and enhances their immunosuppressive functions, thereby contributing to the formation of an immunosuppressive microenvironment.

Previous research has demonstrated an age-related increase in the proportion of γδT cells, particularly γδ17. Our current findings confirmed that aging increases the proportion of γδ17 cells without altering the proportion of γδ1 cells. This finding also demonstrates that aging intensifies the distinctions between mice bearing tumors or not. Remarkably, the substantial disparities in tumor-triggered γδ17 cells were discernible solely among the elderly mice. The accumulation of γδ17 cells is also a component of the premetastatic niche[58]. We also observed an increased proportion of γδT cells in lung and lymph nodes following aging, accompanied by an upregulation in the expression level of IL-17. Previous studies have shown that aging may upregulate IL-7 levels, thereby promoting the entry of γδT cells into the lungs[59]. Our study found that the expression level of S1pr1 was decreased in lung-resident γδT cells and enhanced in lymph nodes γδT cells in aged mice. This suggests a potential retention of lung-resident γδT cells and egression of γδT cells from the lymph nodes, ultimately contributing to the formation of the pre-metastatic niche. Although the proportion of γδT cells was reduced, the expression level of IL-17A in the spleen also exhibited an increased trend during aging. There was no significant difference in the expression of S1pr1. Therefore, the reasons underlying these observations require further investigation. Additionally, the group 3 innate lymphoid cells, another important type of IL-17-producing cell similar to γδ17 and known to enhance anti-tumor immunity[60], were not identified in this study due to the lack of distinct markers and require further research.

Neutrophils demonstrate a two-sided effect, promoting tumorigenesis, while also exerting tumor-inhibitory actions[61]. Our study revealed an increase in the proportion of neutrophils with aging, which is consistent with Angelidis et al[62]. On this basis, we further explored the function of neutrophils and found the upregulation of c-kit+ and active neutrophils. C-kit+ neutrophils exhibit enhanced mitochondrial metabolism and generate higher levels of reactive oxygen species, leading to oxidative DNA damage and promoting cancer development[37,63]. Active neutrophils play a role in driving angiogenesis, remodeling the extracellular matrix, promoting tumor cell proliferation, and contributing to the inflammatory response that facilitates tumor progression[40]. The changes in TLR4 and CD54 may partially account for the increased activity of neutrophils with aging. We speculate that the increased recruitment of immunosuppressive neutrophils may be associated with aging-induced γδ17 cells[64]. Thus, we depleted γδT cells in modeled mice, and observed significant phenotypic changes characterized by a decrease, not only in the overall neutrophil population, but also in c-kit+ and active neutrophils in aged mice. However, no significant changes in the activity or ratio of immunosuppressive neutrophils were observed in young mice. Arginine has been shown to modulate T cell metabolism and participate in cell proliferation[65]. Arginase promotes the metabolism of arginine, limiting its uptake by T cells, and suppressing proliferation and anti-tumor immunity[66]. We observed an age-related increase in Arg2 activity within neutrophils, as evidenced by the higher expression levels of Arg2 in AM mice than in YM. This enhanced arginase activity leads to the suppression of T cell proliferation. Additionally, the inhibitory effect of neutrophils on CD8+ T cells proliferation was reversed by an Arg2 inhibitor, indicating a potential immunosuppressive mechanism for active neutrophils. We also found that age-induced neutrophils increased the expression of PD1 in CD8+ T cells. After neutrophil depletion, the number of lung metastases significantly decreased in aging mice. These results validate our hypothesis: aging triggers an expansion of γδ17 cells, consequently culminating in the recruitment of neutrophils, which wield pro-tumorigenic influence. Notably, the mechanism of neutrophil immunosuppression needs to be further explored.

CD8+ T cells stemness refers to the ability to exhibit stem cell-like behaviors such as self-renewal and pluripotency. This stemness phenotype enables CD8+ T cells to effectively eradicate large metastatic tumors[67]. However, the effect of neutrophils on CD8+ T cells stemness remains unclear. Our study revealed that the depletion of neutrophils in aged mice resulted in increased CD8+ T cells infiltration in the lungs. This was accompanied by an elevated expression of stemness markers (TCF1 and CD62L) and a proliferation marker (Ki67), as well as a decreased proportion of exhausted CD8+ T cells (PD1+TIM3+). Additionally, the depletion of neutrophils enhanced the cytotoxic ability of CD8+ T cells, as indicated by the increased secretion of tumor-killing factors (TNF+IFNγ+) and enhanced degranulation capacity (CD107a+GZMB+). Stem cell-like CD8+ T cells play a crucial role in the rapid expansion of effector T cells following immune checkpoint blockade targeting PD1[68]. These distinguishing

https://doi.org/10.1038/s41467-024-55164-3

features underscore the therapeutic potential of stem cell-like CD8+ T cells in immune checkpoint blockade. Currently, there is no available research on the impact of aging on stem cell-like CD8+ T cells. Our study revealed that aging decreases the stem cell-like CD8+ T cells population through the action of neutrophils, and neutrophil depletion exerts a rescuing effect in this context. Furthermore, these rescue effects of neutrophils depletion may partially depend on PD-L1 and Treg. Interestingly, we found that the same treatment can yield opposite results in young mice, suggesting that the suppression of CD8+ T cells stemness by neutrophils specifically occurs in aging mice, and that neutrophil-depleting therapy may only be beneficial for aged mice.

Fig. 6 | Neutrophils of aged male mice suppress the stemness of CD8+ T cells. Representative images and quantitative results of lung metastases in aged (**a**) and young (**b**) mice with anti-Ly6G or isotype (control) treated. Each group contains six mice. Data expressed as mean ± SD. $P = 8.3E{-}03$ (**a**), $P = 0.63$ (**b**). Significance was determined using an unpaired two-tailed Student's *t* test. $^{**}P < 0.01$, ns $P > 0.05$. **c** Heatmap showing representative GO terms and pathways of CD8+ T cells across AC, YC, AM, and YM groups, calculated by GSVA packages. The color key from white to red indicates expression levels from low to high. **d** MFI of TCF1 in lung CD8+ T cells from AM/AM-anti-Ly6G groups, which were measured by flow cytometry, gated on CD45+CD8+ cells. Each group contains six mice. Data expressed as MFI of TCF1 (mean ± SD). $P = 4.7E{-}03$. Significance was determined using an unpaired two-tailed Student's *t* test. $^{**}P < 0.01$. Flow plots showing the proportions of Ki67+ (**e**), CD62L+CD44− (**f**), PD-1+Tim3+ (**g**), TNF+IFN-γ+ (**h**), GZMB+CD107a+ (**i**) in lung CD8+ T cells from AM anti-Ly6G/control groups measured by flow cytometry, gated on CD45+CD8+ cells. Each group contains six mice. Data expressed as % of Ki67+CD8+, CD62L+CD44-CD8+, PD-1+Tim3+CD8+, TNF+IFN-γ+CD8+, GZMB+CD107a+CD8+ cells (mean ± SD). $P = 0.01$ (**e**), $P = 9.7E{-}03$ (**f**), $P = 0.01$ (**g**), $P = 0.02$ (**h**), $P = 0.03$ (**i**), $P = 8.6E{-}03$ (**k**). Significance was determined using an unpaired two-tailed Student's *t* test. $^{*}P < 0.05$, $^{**}P < 0.01$. **j** UMAP plot of CD8+ T cells subsets from AM and YM groups, and stacked column chart showing the ratio of Stem cell like (PD-1+TCF1+TIM3−) and Exhausted (PD-1+TCF1-TIM3+) CD8+ T cells in AM and YM groups, based on scRNA-seq. The total population is the sum of stem cell-like and exhausted CD8+ T cells. **k** Flow plot showing the proportions of Stem cell like CD8+ T cells in lungs from AM anti-Ly6G/control groups measured by flow cytometry, gated on CD45+CD8+PD-1+ cells. Each group contains six mice. Data expressed as % of stem cell like cells (mean ± SD). Significance was determined using an unpaired two-tailed Student's *t* test. $^{**}P < 0.01$. Source data are provided as a Source Data file.

PCC1, a novel senolytic agent derived from grape seed extract, has been reported to induce mitochondrial dysfunction in senescent cells and selectively trigger apoptosis in these cells, thereby promoting tumor regression and extending lifespan[52]. In our study, the application of PCC1 significantly reduced the number of lung metastatic foci by inhibiting the γδ17-Neutrophil-CD8 axis. The underlying mechanisms may involve the clearance of senescent γδT cells and neutrophils, as well as a decline in PD-L1 expression of neutrophils. This new senolytic agent shows promising potential for treating tumor in aged mice. Nevertheless, research on PCC1 is still limited, and additional experiments are necessary in the future to comprehensively explore its capabilities and mechanisms.

In summary, our study represents an investigation into the role of aging in promoting melanoma metastasis. We employed both a traditional lung metastasis model and an intraocular tumor model to comprehensively explore the impact of aging on metastasis. Leveraging cutting-edge scRNA-seq technology, we delved deep into the alterations within the lung immune microenvironment induced by aging and their consequences for tumor metastasis. Our findings explored the complex relationship between aged immune environment and tumor metastasis, demonstrating that aging can facilitate metastasis by compromising the anti-tumor activity through the γδ17-Neutrophil-CD8 axis. And these age-induced disorders could be partially reversed by PCC1 in mice. However, we exclusively utilized male mice due to their susceptibility to tumor development, as documented in previous research[69,70]. There are notable immunity differences between males and females. Consequently, additional investigations are warranted to examine the immunological differences induced by aging and their implications for tumor metastasis in female animals.

Methods

Mice

The study utilized 2-month-old young, 16-month-old and 20-month-old aged male C57BL/6 J mice obtained from Guangzhou Animal Testing Center. The mice were kept in an environment free of specific pathogens, and their surroundings were carefully controlled, with a 12-hour cycle of light and darkness, a constant temperature of 22 °C, and humidity maintained at levels between 40 to 50%. Experimental mice and control mice were bred separately, and they all had unrestricted access to a chow diet and water. Approval for the animal experiments was granted by the Institutional Animal Care and Use Committee at Zhongshan Ophthalmic Center, Sun Yat-Sen University.

Cells and cell culture

All cells were cultured in a temperature-controlled incubator at 37 °C with a humidified atmosphere containing 5% CO2 and 95% air. Murine melanoma B16F10 cell line was a kind gift from Prof. Yan Hu (Huazhong University of Science and Technology, China). B16F10 were cultured in RPMI 1640 medium supplemented with 10% FBS and 1% penicillin/streptomycin. CD8 + T cells and bone marrow-derived neutrophils were cultured in complete T cell medium. (RPMI 1640 medium containing 10% FBS, 1% penicillin/streptomycin, 1% MEM Non-Essential Amino Acids, 10 mM HEPES, 1 mM Sodium Pyruvate and 0.1% 2-mercaptoethanol). For each specific experimental scale, the cells were seeded at suitable densities.

Establishment of melanoma model

Sub-confluent B16F10 cells were collected through a short trypsin treatment, followed by two washes with PBS. Two groups of mice, 2-month-old and 20-month-old, were used; each group contains six mice in each experiments. For melanoma lung metastatic tumor model, mice received a tail veins injection of 5×10^5 B16F10 cells in 0.2 mL PBS. For orthotopic mouse ocular melanoma model, a 30-gauge needle was carefully inserted near the limbus, passing through the conjunctiva and sclera, and reaching the subretinal space. A blunt needle attached to a 5 µl glass syringe (Hamilton Co., Bonaduz, Switzerland) was then introduced into the subretinal space through the needle track. 2.5×10^5 B16F10 cells in 2 µL suspension was carefully injected into the eyes[71]. Ensuring proper inoculation involved positioning the needle tip inside the eye, preventing tumor cell reflux, and maintaining a clear subconjunctival space without tumor cells throughout the procedure.

Assessment of metastasis

After three weeks of melanoma lung metastatic tumor modeling, mice were euthanized by pentobarbital injection and their lungs were collected after dissection. Lungs were photographed and the number of metastatic foci was recorded per lung. The lungs were then sectioned and fixed, and subsequently subjected to hematoxylin and eosin (HE) staining for micro metastases counts. For orthotopic ocular melanoma modeled mice, tumor-bearing eyes were surgically removed once they attained a diameter of 4 mm. The mice were euthanized 21 days after enucleation. The livers were collected to determine the number of metastatic foci using HE staining. The number of metastatic foci was calculated as the mean number of metastases per 5 random low-power fields (×100). Since the tumor size cannot be measured, the criteria for early end point include rapid or progressive weight loss, anorexia or failure to drink, sizable abdominal enlargement or ascites, lethargy or persistent recumbency, rough hair coat/unkempt appearance/hunched posture, labored breathing, gasping.

The application of procyanidin C1

16-month-old mice were used to administer PCC1 (E0478, selleck), with a dosage of 20 mg/kg intraperitoneally every two weeks. The control group (16-month-old) of mice were injected with an equivalent amount of solvent. After four months of injections, both two groups of mice underwent establishment of melanoma.

Sample collection

After three weeks of tumor modeling, spleens and lymph nodes were collected during mouse dissection, and were grinded for isolated

https://doi.org/10.1038/s41467-024-55164-3

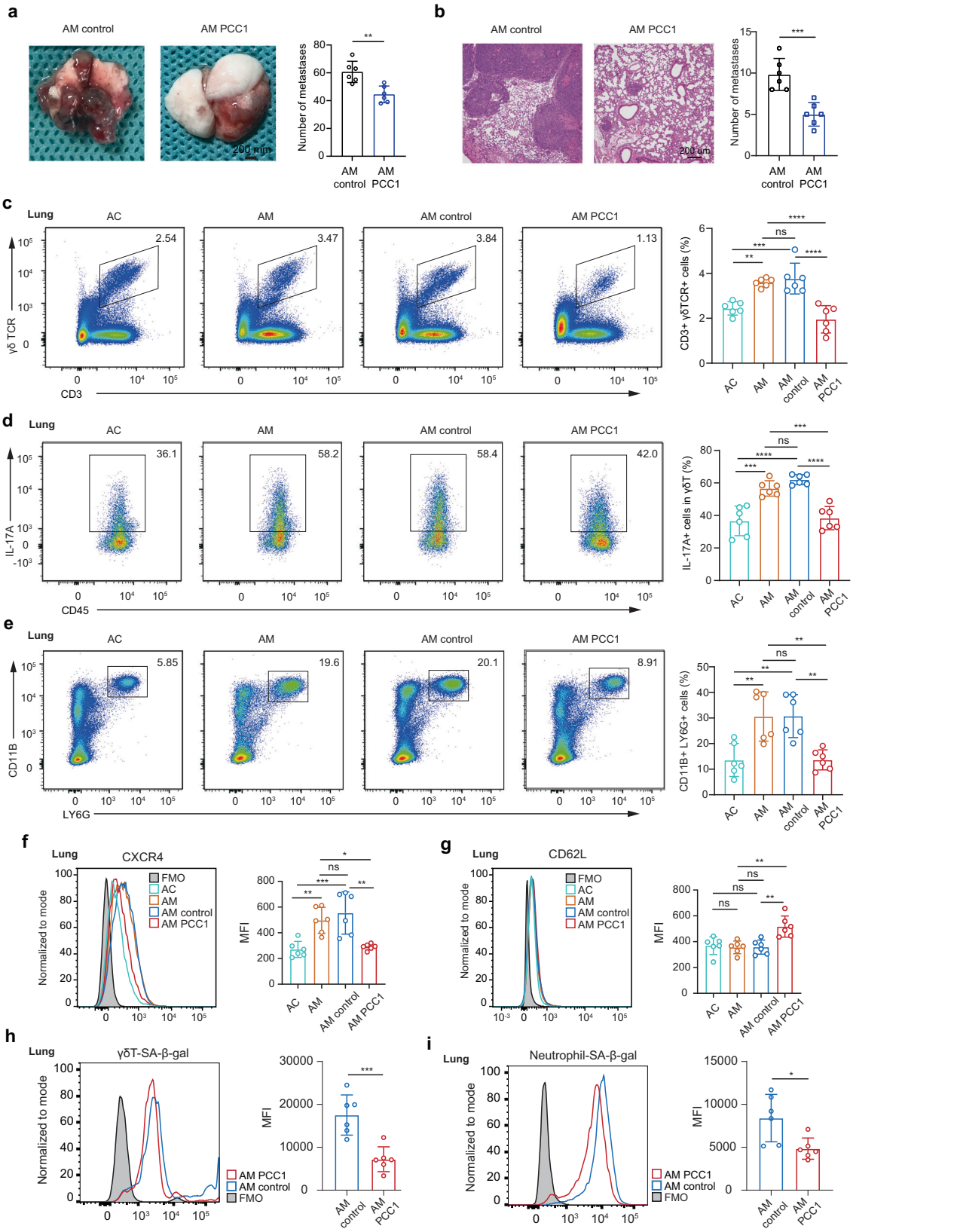

immune cells. Bone marrow cells were isolated by performing an incision at the ends of the leg bones and flushing them out with sterile PBS. Lungs were collected and digested using the Mouse Tumor Dissociation Kit (130-096-730, Miltenyi) and processed with the gentleMACS Dissociator (130-093-235, Miltenyi) following the manufacturer's protocol, for isolating the infiltrated immune cells.

Neutrophils depleting and γδT cells depleting

To delete neutrophils, anti-Ly6G (clone 1A8; BioXCell) was administered intraperitoneally three times a week after modeled (10 mg/kg in InVivoPure pH 7.0 Dilution Buffer)[72]. To deplete γδT cells, anti-γδTCR (clone UC7-13D5; BioXCell) was administered intraperitoneally on days 7, 14, and 21 after modeled (200ug in InVivoPure pH 6.0 T Dilution

Fig. 7 | Procyanidin C1 could reverse the tumor-promoting effect of aging. Four groups, AC mice, AM mice, and AM mice with PCC1 or solvent-treated group, were involved in this part. Each group contains six mice. AM mice were injected PCC1 or solvent from 16 months old. The tumor model was not constructed till 20 months old. PCC1 procyanidin C1. Representative images (**a**) and HE staining (**b**) results of lung metastases. Data expressed as number of metastases (mean ± SD). $P = 2.2E{-}03$ (**a**), $P = 6.0E{-}04$ (**b**). Significance was determined using an unpaired two-tailed Student's *t* test. $^{**}P < 0.01$, $^{***}P < 0.001$. Scale bars: 100 mm (**a**), 200 um (**b**). Proportions of γδT cells (**c**), γδ17 cells (**d**), and neutrophils (**e**) in the lung measured by flow cytometry, gated on CD45+ cells, CD45+CD3+γδTCR+ cells, and CD45+ cells, respectively. Data expressed as % of γδT cells, γδ17 cells, and neutrophils (mean ± SD). **c** AC-AM ($P = 3.1E{-}03$), AC-AM control ($P = 7.7E{-}04$), AM-AM PCC1 ($P = 6.5E{-}05$), AM control-AM PCC1 ($P = 1.7E{-}05$). **d** AC-AM ($P = 1.5E{-}04$), AC-AM control ($P = 6.7E{-}06$), AM-AM PCC1 ($P = 4.4E{-}04$), AM control-AM PCC1 ($P = 1.8E{-}05$). **e** AC-AM ($P = 3.8E{-}03$), AC-AM control ($P = 3.5E{-}03$), AM-AM PCC1 ($P = 3.9E{-}03$), AM control-AM PCC1 ($P = 3.6E{-}03$). Significance was determined using one-way ANOVA. $^{**}P < 0.01$, $^{****}P < 0.0001$, ns $P > 0.05$. MFI of CXCR4 (**f**) and CD62L (**g**) in lung neutrophils measured by flow cytometry, gated on CD45+CD11B+LY6G+ cells. Data expressed as MFI of CXCR4 and CD62L (mean ± SD). **f** AC-AM ($P = 5.0E{-}03$), AC-AM control ($P = 5.6E{-}04$), AM-AM PCC1 ($P = 0.01$), AM control-AM PCC1 ($P = 1.2E{-}03$). **g** AM-AM PCC1 ($P = 1.8E{-}03$), AM control-AM PCC1 ($P = 2.0E{-}03$). Significance was determined using one-way ANOVA. $^{*}P < 0.05$, $^{**}P < 0.01$, ns $P > 0.05$. MFI of SA-β-gal in γδT (**h**) and neutrophils (**i**) in lungs measured by flow cytometry, gated on CD45+CD3+γδTCR+ or CD45+CD11B+LY6G+ cells. Each group contains six mice. Data expressed as MFI of SA-β-Gal (mean ± SD). $P = 1.0E{-}03$ (**h**), $P = 0.02$ (**i**). Significance was determined using unpaired two-tailed Student's *t* test. $^{***}P < 0.001$, $^{**}P < 0.05$. Source data are provided as a Source Data file.

Buffer)[73]. The control group of mice was administered equivalent volumes of antibodies with isotype control.

Flow cytometric analysis

The cells underwent staining using a live/dead dye (BioLegend, 423105) for 10 minutes at 4 °C. Antibodies specific to surface markers included CD45 (BioLegend, 103138, 0.2 μg/ml), CD3 (BioLegend, 100232, 100206, 100228, 0.2 μg/ml), CD4 (BioLegend, 100434, 0.2 μg/ml), CD8 (BioLegend, 100753, 100751, 100733, 100708, 0.2 μg/ml), γδTCR (BioLegend, 118119, 118108, 0.2 μg/ml), CD62L (BioLegend, 104406, 0.2 μg/ml), CD44 (BioLegend, 103012, 103047, 0.2 μg/ml), PD-1 (BioLegend, Cat#135215, 135205, 135207, 0.2 μg/ml), CD11b (BioLegend, 101205, 101257, 0.2 μg/ml), Ly-6G (BioLegend, 127643, 127614, 0.2 μg/ml), CXCR4 (BioLegend, 146505, 0.2 μg/ml), CXCR2 (BioLegend, 149315, 0.2 μg/ml), C-kit (BioLegend, 105811, 0.2 μg/ml), TIM-3 (BioLegend, 119723, 0.2 μg/ml), S1PR1 (R&D, FAB7-89A, 0.2 μg/ml), CD69 (BioLegend, 104507, 0.2 μg/ml), CD107a (BioLegend, 121617, 0.2 μg/ml), TLR2 (BioLegend, 153011, 0.2 μg/ml), TLR4 (BioLegend, 117605, 0.2 μg/ml), CD54 (BioLegend, 116119, 0.2 μg/ml), PDL1 (BioLegend, 124313, 0.2 μg/ml), SA-β-GAL (abcam,ab228562). Before detecting intracellular cytokines, the cells were stimulated with phorbol myristate acetate (5 ng/mL, Sigma), brefeldin A (1 μg/mL, Sigma), and ionomycin (500 ng/mL, Sigma) at 37 °C for 4 hours. Intracellular antibodies included IL-17A (BioLegend, 506930, 506912, 0.2 μg/ml), GZMB (BioLegend, 372213, 0.2 μg/ml), IFNγ (BioLegend, 505835, 0.2 μg/ml), Ki-67 (BioLegend, 652408, 652413, 0.2 μg/ml), TNF (BioLegend, 506306, 0.2 μg/ml), TCF-1 (BD Pharmingen, 564217, 0.2 μg/ml), Arg1 (CST, 93668S, 0.2 μg/ml), Arg2 (CST, 55003S, 0.2 μg/ml), P53 (Bioss, bs-2090R, 0.2 μg/ml), FOXP3 (Invitrogen, 11-5773-82, 0.2 μg/ml). Labeled cells were analyzed through a flow cytometer (BD LSRFortessa, USA). FlowJo software (version 10.0.7, Tree Star, Ashland, OR, USA) was used for data evaluation and analysis. Gates were set by FMO controls; detailed gating strategies were provided in Supplementary Figs. 17 and 18. The quantity of cell types was counted for every 0.1 g of lung tissue. All the dilution ratio of antibody was 1:500.

Co-culture of neutrophils with CD8+ T cells

Neutrophils were sorted from bone marrows of YM or AM mice by mouse neutrophil isolation kit (STEMCELL Technologies, BC, Canada). CD8+ T cells were extracted from the spleen of YC mice using mouse CD8 + T cell isolation kit (STEMCELL Technologies, BC, Canada). The CD8 + T cells sorted by magnetic beads were stimulated by anti-CD3/28 beads (Gibco) at a ratio of 1:5 (1 ml beads per 4×10^4 cells). Equal numbers ($2{\times}10^5$) of neutrophils from YM or AM mice and CD8 + T cells were then co-cultured in 96-well plate for 2 days. During co-culture, two conditions were tested: with or without the presence of Arg2 inhibitor BEC (500 μM, MCE company). After 2 days of co-culture, the cells from the cultures were collected. Cells were harvested for flow cytometry assays.

Enzyme-linked immunosorbent assay

Supernatant obtained after culturing neutrophils for 2 days and mouse serum were analyzed using the Arg2 enzyme-linked immunosorbent assay kit (WED796Hu, Cloud-clone, Wuhan, China) following the manufacturer's instructions. These kits provide specific assays for quantifying Arg2 levels.

Single-cell collection for scRNA-seq

Lungs were digested as before. Red blood cells were eliminated from the sample using Red Blood Cell Lysing Buffer (Sigma). CD45+ cells were isolated using a mouse CD45+ cells isolation kit (STEMCELL Technologies, BC, Canada) and flow sorting. The sorted cells were collected and filtered using a 70 μm cell filter. Cells were sent for sequencing with a minimum viability of 85%. Subsequently, these cells were converted into barcoded scRNA-seq libraries using 10x Genomics for subsequent analyses. Initial data processing was performed using CellRanger software and the Seurat package. Harmony package was used to eliminate batch effects among the four groups.

scRNA-seq library preparation

The scRNA-seq libraries were generated using the Chromium Single Cell 5′ Library and Gel Bead Kit (10x Genomics, 120237) in accordance with the guidelines provided by the manufacturer, with minor adjustments made to the protocol. First, cells were washed with 0.04% BSA buffer (50 mL deionized PBS containing 0.02 g BSA) and subsequently captured in droplets. Subsequently, a series of sequential steps, including reverse transcription, emulsion breaking, barcoded-cDNA purification using Dynabeads, and PCR amplification, were carried out. The amplified cDNA was utilized for constructing the 5′ gene expression library. In particular, the 50 ng of amplified cDNA underwent fragmentation and end-repair, and then underwent double-size selection utilizing SPRIselect beads. The library was then subjected to sequencing on the NovaSeq platform (Illumina NovaSeq6000) to generate 150c bp paired-end reads.

Analysis of scRNA-seq data

The initial data, represented as fastq files, were obtained by processing the Raw BCL files through Illumina bcl2fastq converter. For the primary quality assessment, the FastQC software was utilized. The following factors were assessed: (1) the number of occurrences of "N" bases should not exceed 3; (2) the proportion of bases with a quality value below 5 should not exceed 20%; and (3) adapter sequences were removed. All subsequent analyses were conducted using the cleaned data, ensuring high quality.

To demultiplex and barcode the sequences obtained from the NovaSeq system, the "cellranger count" command from the CellRanger Software Suite (version 7.1.0) (https://www.10xgenomics.com/support/software/cell-ranger/latest/tutorials/cr-tutorial-ct) was employed. To create the single-cell expression matrix, the Seurat software (version 3.2.0) (https://satijalab.org/seurat/articles/pbmc3k_

tutorial) was utilized. The Seurat package was instrumental in conducting multiple procedures, encompassing data filtration, normalization, dimensionality reduction, cluster analysis, and exploration of differentially expressed genes[74]. Cells that exhibited a number of expressed genes less than 200 or greater than 4000 were excluded. Furthermore, cells displaying a mitochondrial gene ratio surpassing 10% were excluded from the analysis. Then filter out red blood cells with high expression of Hbb-a1 and Hbb-bs genes. The Harmony package (version 0.1.1) (https://satijalab.org/seurat/reference/harmonyintegration) was utilized, following the approach described by Korsunsky, to address the batch effect present in different samples.

Dimensionality reduction and clustering analysis

In the analysis of scRNA-seq data using Seurat, the data underwent normalization using the "NormalizeData" function. Next, the top 2000 variable genes underwent principal component analysis (PCA) using the "FindVariableGenes" function with default settings. To cluster the cells, the "FindClusters" function was employed. Visualization of the clustered cells was achieved using the "RunUMAP" function, which utilizes a 2-dimensional UMAP algorithm. Moreover, marker genes linked to distinct clusters were identified using the "FindAllMarkers" function, employing default parameters.

DEG analysis

For differential expression analysis of various cell types between different groups, the "FindMarkers" function was employed (adjusted *p*-value threshold of <0.05 and |Log2FC | > 0.25). Before proceeding with the DEG analysis, cell types with either insufficient representation or less than three cells in the comparison groups were excluded from further analysis. Gene expression was calculated using the LogNormalize and z-score algorithms built into the Seurat package.

Gene set functional enrichment analysis

To perform gene ontology (GO) (https://metascape.org/gp/#/main/step1) and pathway enrichment analysis, we employed the Metascape webtool (www.metascape.org), following the methodology outlined by Zhou. To conduct gene set variation analysis, we utilized the GSVA package (version 1.42.0). (https://www.bioconductor.org/packages/devel/bioc/vignettes/GSVA/inst/doc/GSVA.html) The ggplot2 package (version 3.4.1), was used for visualization.

Cell-cell communication analysis

Intercellular communication analysis was carried out using CellPhoneDB (version 3.0.0) (https://github.com/ventolab/CellphoneDB) and CellChat package (version 1.4.0) (https://github.com/jinworks/CellChat). Ligand-receptor pairs were selected and analyzed, considering only those pairs that were present in more than 10% of a given cell type. A comparison of mean expression levels for ligand-receptor pairs was carried out among various cell types. Pairs with a *p*-value less than 0.05 were chosen for further computational analysis of intercellular communication.

Transcriptional factor analysis

Using scRNA-seq data, the SCENIC (version 1.3.1) (https://htmlpreview.github.io/?https://github.com/aertslab/SCENIC/blob/master/inst/doc/SCENIC_Running.html) workflow was employed to predict core regulatory transcription factors. Gene regulatory networks between the aged and young groups were inferred using the GENIE3 package. The RcisTarget package, based on the mm9 RcisTarget database, was employed to identify top regulons. Additionally, the AUCell package was used to assess the activity of regulons. Data were normalized using Z-score algorithm to calculate the expression levels of regulons among different cell types. The visualization of transcription factor targets with high-confidence annotation was achieved using Cytoscape (version 3.8.2).

Pseudotime analysis

Pseudotime analysis was conducted using the Monocle2 package (version 2.22.0) (https://cole-trapnell-lab.github.io/monocle-release/docs/). To ascertain the gene ordering, a threshold for expression in at least 10 cells was implemented. The ordering was determined based on a combination of intercluster differential expression and dispersion, with a q-value cutoff of less than 0.1. The DDRTree dimensionality reduction algorithm was utilized to visualize the trajectory structure in a 2-dimensional space, with cells ordered along the pseudotime trajectory.

Statistical analysis

GraphPad Prism Software (version 8.4.0) was employed for data analysis and presentation. The data is presented as the mean values accompanied by their standard deviation (mean ± SD). For statistical analysis, either an unpaired, two-tailed Student's *t* test or one-way ANOVA was chosen, depending on the experimental design. The statistical significance was indicated using the following notation for interpretation: $P \le 0.0001$ = ****; $0.0001 < P \le 0.001$ = ***; $0.001 < P \le 0.01$ = **; $0.01 < P \le 0.05$ = *; $P > 0.05$ = ns = not significant.

Reporting summary

Further information on research design is available in the Nature Portfolio Reporting Summary linked to this article.

Data availability

The scRNA-seq sequencing data generated in this study have been deposited in the Genome Sequence Archive (GSA, BIG, https://bigd.big.ac.cn/gsa/) under project number (PRJCA024149) and GSA accession number (mouse data: CRA015263). Source data are provided with this paper.

References

1. Fane, M. & Weeraratna, A. T. Normal aging and its role in cancer metastasis. *Cold Spring Harb. Perspect. Med.* **10**, a037341 (2020).
2. Siegel, R. L., Miller, K. D., Fuchs, H. E. & Jemal, A. Cancer statistics, 2022. *CA Cancer J. Clin.* **72**, 7–33 (2022).
3. López-Otín, C., Pietrocola, F., Roiz-Valle, D., Galluzzi, L. & Kroemer, G. Meta-hallmarks of aging and cancer. *Cell Metab.* **35**, 12–35 (2023).
4. Fane, M. & Weeraratna, A. T. How the ageing microenvironment influences tumour progression. *Nat. Rev. Cancer* **20**, 89–106 (2020).
5. López-Otín, C., Blasco, M. A., Partridge, L., Serrano, M. & Kroemer, G. The hallmarks of aging. *Cell* **153**, 1194–1217 (2013).
6. Leonardi, G. C., Accardi, G., Monastero, R., Nicoletti, F. & Libra, M. Ageing: from inflammation to cancer. *Immun. Ageing* **15**, 1 (2018).
7. Palmer, D. B. The effect of age on thymic function. *Front. Immunol.* **4**, 316 (2013).
8. Li, H. et al. Aging weakens Th17 cell pathogenicity and ameliorates experimental autoimmune uveitis in mice. *Protein Cell* **13**, 422–445 (2022).
9. Huang, Z. et al. Effects of sex and aging on the immune cell landscape as assessed by single-cell transcriptomic analysis. *Proc. Natl Acad. Sci. USA* **118**, e2023216118 (2021).
10. Miller, A. J. & Mihm, M. C. Jr Melanoma. *N. Engl. J. Med.* **355**, 51–65 (2006).
11. Elvin, P. & Evans, C. W. Cell adhesion and experimental metastasis: a study using the B16 malignant melanoma model system. *Eur. J. Cancer Clin. Oncol.* **20**, 107–114 (1984).
12. Ashur-Fabian, O. et al. Tetrac delayed the onset of ocular melanoma in an orthotopic mouse model. *Front. Endocrinol.* **9**, 775 (2018).
13. Wu, C. F. et al. The lack of type I interferon induces neutrophil-mediated pre-metastatic niche formation in the mouse lung. *Int. J. Cancer* **137**, 837–847 (2015).

14. Franklin, R. A. et al. The cellular and molecular origin of tumor-associated macrophages. *Science* **344**, 921–925 (2014).
15. Lin, E. Y. & Pollard, J. W. Tumor-associated macrophages press the angiogenic switch in breast cancer. *Cancer Res.* **67**, 5064–5066 (2007).
16. Leone, R. D. & Powell, J. D. Metabolism of immune cells in cancer. *Nat. Rev. Cancer* **20**, 516–531 (2020).
17. Maier, B. et al. A conserved dendritic-cell regulatory program limits antitumour immunity. *Nature* **580**, 257–262 (2020).
18. Chiba, S. et al. Recognition of tumor cells by Dectin-1 orchestrates innate immune cells for anti-tumor responses. *Elife* **3**, e04177 (2014).
19. van der Feen, D. E. et al. Cellular senescence impairs the reversibility of pulmonary arterial hypertension. *Sci. Transl. Med.* **12**, eaaw4974 (2020).
20. Yang, F. et al. Cyclophosphamide loaded thermo-responsive hydrogel system synergize with a hydrogel cancer vaccine to amplify cancer immunotherapy in a prime-boost manner. *Bioact. Mater.* **6**, 3036–3048 (2021).
21. Patil, R. S. et al. IL17 producing γδT cells induce angiogenesis and are associated with poor survival in gallbladder cancer patients. *Int. J. Cancer* **139**, 869–881 (2016).
22. Mills, K. H. Induction, function and regulation of IL-17-producing T cells. *Eur. J. Immunol.* **38**, 2636–2649 (2008).
23. Wang, Q. et al. Tumor evolution of glioma-intrinsic gene expression subtypes associates with immunological changes in the microenvironment. *Cancer Cell* **32**, 42–56.e46 (2017).
24. McNamee, K. E. et al. IL-17 induces hyperalgesia via TNF-dependent neutrophil infiltration. *Pain* **152**, 1838–1845 (2011).
25. Choi, Y. et al. Nanocages displaying SIRP gamma clusters combined with prophagocytic stimulus of phagocytes potentiate antitumor immunity. *Cancer Gene Ther.* **28**, 960–970 (2021).
26. Sasaki, S. et al. Essential roles of the interaction between cancer cell-derived chemokine, CCL4, and intra-bone CCR5-expressing fibroblasts in breast cancer bone metastasis. *Cancer Lett.* **378**, 23–32 (2016).
27. Liang, Y. et al. Single-cell analysis reveals hypoxia-induced immunosuppressive microenvironment in intrahepatic cholangiocarcinoma. *Biochim. Biophys. Acta Mol. Basis Dis.* **1870**, 167276 (2024).
28. Gassner, F. J. et al. Chronic lymphocytic leukaemia induces an exhausted T cell phenotype in the TCL1 transgenic mouse model. *Br. J. Haematol.* **170**, 515–522 (2015).
29. Yu, M., Scherwitzl, I., Opp, S., Tsirigos, A. & Meruelo, D. Molecular and metabolic pathways mediating curative treatment of a non-Hodgkin B cell lymphoma by Sindbis viral vectors and anti-4-1BB monoclonal antibody. *J. Immunother. Cancer* **7**, 185 (2019).
30. Shiow, L. R. et al. CD69 acts downstream of interferon-alpha/beta to inhibit S1P1 and lymphocyte egress from lymphoid organs. *Nature* **440**, 540–544 (2006).
31. McGinley, M. P. & Cohen, J. A. Sphingosine 1-phosphate receptor modulators in multiple sclerosis and other conditions. *Lancet* **398**, 1184–1194 (2021).
32. Alves de Lima, K. et al. Meningeal γδ T cells regulate anxiety-like behavior via IL-17a signaling in neurons. *Nat. Immunol.* **21**, 1421–1429 (2020).
33. Mensurado, S., Blanco-Domínguez, R. & Silva-Santos, B. The emerging roles of γδ T cells in cancer immunotherapy. *Nat. Rev. Clin. Oncol.* **20**, 178–191 (2023).
34. Nakazawa, D. & Kudo, T. Novel therapeutic strategy based on neutrophil subset and its function in autoimmune disease. *Front. Pharm.* **12**, 684886 (2021).
35. Bäck, M. et al. International Union of Basic and Clinical Pharmacology. LXXXIV: leukotriene receptor nomenclature, distribution, and pathophysiological functions. *Pharm. Rev.* **63**, 539–584 (2011).
36. Wu, L. et al. IL-17-CXC chemokine receptor 2 axis facilitates breast cancer progression by up-regulating neutrophil recruitment. *Am. J. Pathol.* **190**, 222–233 (2020).
37. Rice, C. M. et al. Tumour-elicited neutrophils engage mitochondrial metabolism to circumvent nutrient limitations and maintain immune suppression. *Nat. Commun.* **9**, 5099 (2018).
38. Svensmark, J. H. & Brakebusch, C. Rho GTPases in cancer: friend or foe? *Oncogene* **38**, 7447–7456 (2019).
39. Srinivas, U. S., Tan, B. W. Q., Vellayappan, B. A. & Jeyasekharan, A. D. ROS and the DNA damage response in cancer. *Redox Biol.* **25**, 101084 (2019).
40. Jaillon, S. et al. Neutrophil diversity and plasticity in tumour progression and therapy. *Nat. Rev. Cancer* **20**, 485–503 (2020).
41. Yang, C. et al. Aged neutrophils form mitochondria-dependent vital NETs to promote breast cancer lung metastasis. *J. Immunother. Cancer* **9**, e002875 (2021).
42. Filippi, M. D., Szczur, K., Harris, C. E. & Berclaz, P. Y. Rho GTPase Rac1 is critical for neutrophil migration into the lung. *Blood* **109**, 1257–1264 (2007).
43. Zhang, D. et al. Neutrophil ageing is regulated by the microbiome. *Nature* **525**, 528–532 (2015).
44. Chu, D. K. et al. T helper cell IL-4 drives intestinal Th2 priming to oral peanut antigen, under the control of OX40L and independent of innate-like lymphocytes. *Mucosal Immunol.* **7**, 1395–1404 (2014).
45. Rodriguez, P. C. et al. Arginase I production in the tumor microenvironment by mature myeloid cells inhibits T-cell receptor expression and antigen-specific T-cell responses. *Cancer Res.* **64**, 5839–5849 (2004).
46. Moses, K. et al. Survival of residual neutrophils and accelerated myelopoiesis limit the efficacy of antibody-mediated depletion of Ly-6G+ cells in tumor-bearing mice. *J. Leukoc. Biol.* **99**, 811–823 (2016).
47. Jansen, C. S. et al. An intra-tumoral niche maintains and differentiates stem-like CD8 T cells. *Nature* **576**, 465–470 (2019).
48. Yang, C. et al. Androgen receptor-mediated CD8(+) T cell stemness programs drive sex differences in antitumor immunity. *Immunity* **55**, 1268–1283.e1269 (2022).
49. Xue, R. et al. Liver tumour immune microenvironment subtypes and neutrophil heterogeneity. *Nature* **612**, 141–147 (2022).
50. Wang, H. et al. Regulatory T-cell and neutrophil extracellular trap interaction contributes to carcinogenesis in non-alcoholic steatohepatitis. *J. Hepatol.* **75**, 1271–1283 (2021).
51. Wherry, E. J. & Kurachi, M. Molecular and cellular insights into T cell exhaustion. *Nat. Rev. Immunol.* **15**, 486–499 (2015).
52. Xu, Q. et al. The flavonoid procyanidin C1 has senotherapeutic activity and increases lifespan in mice. *Nat. Metab.* **3**, 1706–1726 (2021).
53. Triana-Martínez, F. et al. Identification and characterization of cardiac glycosides as senolytic compounds. *Nat. Commun.* **10**, 4731 (2019).
54. Fane, M. E. et al. Stromal changes in the aged lung induce an emergence from melanoma dormancy. *Nature* **606**, 396–405 (2022).
55. Ecker, B. L. et al. Age-related changes in HAPLN1 increase lymphatic permeability and affect routes of melanoma metastasis. *Cancer Discov.* **9**, 82–95 (2019).
56. Kaur, A. et al. sFRP2 in the aged microenvironment drives melanoma metastasis and therapy resistance. *Nature* **532**, 250–254 (2016).
57. Ma, S. et al. Single-cell transcriptomic atlas of primate cardiopulmonary aging. *Cell Res.* **31**, 415–432 (2021).
58. Liu, Y. & Cao, X. Characteristics and significance of the pre-metastatic niche. *Cancer Cell* **30**, 668–681 (2016).

59. Chen, H. C. et al. IL-7-dependent compositional changes within the γδ T cell pool in lymph nodes during ageing lead to an unbalanced anti-tumour response. *EMBO Rep.* **20**, e47379 (2019).
60. Castillo-González, R., Valle-Noguera, A., Gomez-Sánchez, M. J., Xia, P. & Cruz-Adalia, A. Innate lymphoid cells type 3 in cancer. *Front. Immunol.* **13**, 1033252 (2022).
61. Giese, M. A., Hind, L. E. & Huttenlocher, A. Neutrophil plasticity in the tumor microenvironment. *Blood* **133**, 2159–2167 (2019).
62. Angelidis, I. et al. An atlas of the aging lung mapped by single cell transcriptomics and deep tissue proteomics. *Nat. Commun.* **10**, 963 (2019).
63. Güngör, N. et al. Genotoxic effects of neutrophils and hypochlorous acid. *Mutagenesis* **25**, 149–154 (2010).
64. Zhang, Z. et al. "γδT Cell-IL17A-Neutrophil" axis drives immunosuppression and confers breast cancer resistance to high-dose anti-VEGFR2 therapy. *Front. Immunol.* **12**, 699478 (2021).
65. Geiger, R. et al. L-arginine modulates T cell metabolism and enhances survival and anti-tumor activity. *Cell* **167**, 829–842.e813 (2016).
66. Li, X. et al. Navigating metabolic pathways to enhance antitumour immunity and immunotherapy. *Nat. Rev. Clin. Oncol.* **16**, 425–441 (2019).
67. Vodnala, S. K. et al. T cell stemness and dysfunction in tumors are triggered by a common mechanism. *Science* **363**, eaau0135 (2019).
68. Kallies, A., Zehn, D. & Utzschneider, D. T. Precursor exhausted T cells: key to successful immunotherapy? *Nat. Rev. Immunol.* **20**, 128–136 (2020).
69. Liu, B. et al. Interrogation of gender disparity uncovers androgen receptor as the transcriptional activator for oncogenic miR-125b in gastric cancer. *Cell Death Dis.* **12**, 441 (2021).
70. Cao, B. et al. Inhibition of androgen receptor enhanced the anticancer effects of everolimus through targeting glucose transporter 12. *Int. J. Biol. Sci.* **19**, 104–119 (2023).
71. Dithmar, S. A., Rusciano, D. A., Armstrong, C. A., Lynn, M. J. & Grossniklaus, H. E. Depletion of NK cell activity results in growth of hepatic micrometastases in a murine ocular melanoma model. *Curr. Eye Res.* **19**, 426–431 (1999).
72. Faget, J. et al. Neutrophils and snail orchestrate the establishment of a pro-tumor microenvironment in lung cancer. *Cell Rep.* **21**, 3190–3204 (2017).
73. Wu, H. et al. Depletion of gammadelta T cells exacerbates murine adriamycin nephropathy. *J. Am. Soc. Nephrol.* **18**, 1180–1189 (2007).
74. Butler, A., Hoffman, P., Smibert, P., Papalexi, E. & Satija, R. Integrating single-cell transcriptomic data across different conditions, technologies, and species. *Nat. Biotechnol.* **36**, 411–420 (2018).

Acknowledgements

This study was supported by the National Outstanding Youth Science Fund Project of China (No. 82122016) [W.S.] and Municipal School (Hospital) Jointly Fund Project of Guang Zhou (2023A03J0176) [W.S.] and China Postdoctoral Science Foundation (2024T171071 and 2023M744017) [R.D.]. We thank the professor Yan Hu (Union Hospital, Tongji Medical College, Huazhong University of Science and Technology) for her kindly instruction. We thank the staff of Laboratory Animal Center at State Key Laboratory of Ophthalmology, Zhongshan Ophthalmic Center for technical support.

Author contributions

W.S., X.F., and R.J. designed research; R.D., L.J., and T.W. performed research; R.D., L.J., T.W., Z.L., X.Y., and Y.G. analyzed data; R.D. and L.J. wrote the paper.

Competing interests

The authors declare no competing interests.

Additional information

Supplementary information The online version contains supplementary material available at https://doi.org/10.1038/s41467-024-55164-3.

Correspondence and requests for materials should be addressed to Renbing Jia, Xianqun Fan or Wenru Su.

Peer review information *Nature Communications* thanks Jing-Dong Han, Sigrid Hatse, Shirin Kalyan and the other, anonymous, reviewer(s) for their contribution to the peer review of this work. A peer review file is available.